Enhancement of flow boiling heat transfer using heterogeneous wettability patterned surfaces with varying inter-spacing.

Wei-Ting Hsu*, Donghwi Lee[¥], Namkyu Lee[#], Maroosol Yun* and Hyung Hee Cho*,[†]

* Department of Mechanical Engineering, Yonsei University, 50 Yonsei-ro, Seodaemun-gu, Seoul 120-749, Korea

¥ Department of Mechanical Engineering, University of Wisconsin–Madison, 1500 Engineering Drive, Madison, WI 53706, United States

#IBI-4, Forschungszentrum Jülich GmbH, D-52428 Jülich, Germany

†Corresponding author: hhcho@yonsei.ac.kr (H. H. Cho)

Abstract

This study experimentally investigated the influence of heterogeneous wettability-patterned surfaces with varying inter-spacing on flow boiling heat transfer characteristics. The test surfaces consisted of three fluorooctyltrichlorosilane hydrophobic-patterned array structures having a triangle, inverted triangle, and circular shape on a SiO_2- hydrophilic substrate, with an inter-spacing of 0.75 or 1 mm. The working fluid was deionized water, and the Reynolds number was 6,000 at atmospheric pressure. Among the test surfaces, varying the inter-spacing between neighboring hydrophobic patterns slightly enhanced the heat transfer coefficient (HTC) due to changing the bubble characteristics. In terms of the shape effect of hydrophobic patterns, the heterogeneous wettability-patterned surfaces dominated the overall flow boiling heat transfer performance showing a significant increase in critical heat flux (CHF) compared to the Si surface, by 40–43%. In addition, all of the wettability test surfaces showed a markedly higher heat transfer coefficient than the Si surface, by 35–163%. This experiment is explained by analyzing the relationship between bubble lift forces and the various hydrophobic-patterned shapes in a horizontal flow channel, in an attempt to better understand flow boiling heat transfer and optimize the pattern design.

Keywords:

Flow boiling heat transfer; Shape effect of hydrophobic patterned arrays; Wettability-patterned surface; Bubble visualization

Nomenclature

A	=	Area (m^2)
a	=	Location of hydrophobic pattern
b	=	Calibration coefficient
D	=	Departure diameter (mm)
F	=	Surface tension force (N)
h	=	Heat transfer coefficient ($W/m^2 \cdot K$)
I	=	Current (A)
k	=	Thermal conductivity (W/m·K)
L	=	Length (m)
l	=	Thickness of RTD sensor
Q	=	Total input heat (W)
q	=	Heat flux (W/m^2)
q_{loss}	=	Loss heat (W/m^2)
Re	=	Reynolds number
r	=	Distance in polar coordinates
P	=	Inter-spacing between neighboring hydrophobic patterns (mm)
T	=	Temperature (°C)
t	=	Thickness (m)
V	=	Input voltage to the ITO heater (V)
Greek letter		
α	=	Advancing contact angle (°)
β	=	Receding contact angle (°)
γ	=	General contact angle
θ	=	Static contact angle (°)
σ	=	Surface tension (N/m)

υ	=	Shape parameter
φ	=	Polar angle around bubble
χ	=	Standard deviation

Subscripts

b	=	Bubble
c	=	Contact
e	=	Entrance
f	=	Fluid
sx	=	Surface tension force in the x-direction
sy	=	Surface tension force in the y-direction
W	=	Heated wall

1. Introduction

In recent years, thermal management issues have attracted increasing interest in industrial applications, as the average output heat generated by a target cannot be released efficiently into the cooling fluid, thereby reducing the lifetime of commercial products and increasing operating costs. Boiling heat transfer is an efficient cooling mechanism, as the cooling method for power integrated circuit packages used in electric vehicles, compact electric power generators, and electronic miniaturization; this transfer process works via bubble-induced agitation in the superheated liquid layer, and offers an efficient means of heat dissipation for preventing the operating units from malfunctioning [1-4].

Surface wettability is among the most important of the various parameters that could be modified to enhance boiling heat transfer performance in pool [5, 6] or flow boiling [7, 8]. In terms of hydrophobic surfaces, bubble nucleation becomes more active on the heating surface at low superheat, which can promote the onset of nucleation boiling and enhance the heat transfer coefficient (HTC). In other words, hydrophilic surfaces can supply more cooling liquid to the surface to prevent rapid bubble coalescence and premature dry-out, thus delaying critical heat flux (CHF).

To take advantage of both hydrophobic and hydrophilic surfaces and thus achieve high-boiling heat transfer performance, several research groups have created surfaces with two wettability contrast regions. Betz et al. [9, 10] used an experimental method to examine the effect of surface wettability on pool boiling characteristics on surfaces that combined a hydrophilic substrate with hydrophobic-patterned arrays, i.e., so-called *biphilic* surfaces. Their experimental results showed that the test surfaces with hydrophobic- and hydrophilic-coated layers enhanced the HTC and CHF by 100% and 65%, respectively, compared to a homogeneous hydrophilic surface (static contact angle: $\theta_c = 7°$). Thus, the remarkable improvement in pool boiling heat transfer performance was attributed to manipulation of surface wettability. Similar trends in surface wettability have been observed in previous studies [11, 12]. In addition, bubble behavior also plays an important role in improving the HTC and CHF, depending on the surface wettability [13-16].

More recently, several studies have focused on surfaces with hydrophobic networks and a hydrophilic substrate for enhancing boiling performance, where the bubble behavior on the heating surface depended on the disparity between the number and size of hydrophobic patterns; in these studies, the inter-spacing between two neighboring patterns was emphasized as a

noteworthy factor improving the heat transfer characteristics under pool boiling conditions [17-21]. Regarding the hydrophobic-patterned array design on the hydrophilic surface, a large number of hydrophobic patterns with a relatively small size resulted in a high density of bubble nucleation, owing to bubbles that only formed on surfaces with hydrophobicity, thereby improving the heat dissipation capacity under low superheating conditions. In contrast, a high nucleation site density of bubbles could worsen boiling performance, by inhibiting efficient mixing within the boundary layer near the heating surface under an exponentially escalating heat flux [17]. For a surface consisting of hydrophobic-patterned arrays with favorable inter-spacing between each pattern, bubbles that form on a wettability-patterned surface could become more active in comparison to bubbles that form on a surface with relatively small inter-spacing, leading to a significant enhancement in HTC, especially in the low heat flux regime [18]. This suggests that the number of hydrophobic patterns influences the high heat flux regime, whereas inter-spacing between neighboring patterns is the dominant factor in boiling heat transfer in the low heat flux regime. However, bubble coalescence controls boiling heat transfer with respect to wettability-patterned surfaces. In a study by Sujith et al. [21], surfaces were fabricated with Teflon hydrophobic networks on a SiO_2- hydrophilic surface; the surface with a 2-mm square pattern and 5-mm inter-spacing demonstrated the highest boiling heat transfer performance. Based on these results, they suggested a distance of 3.12 mm between hydrophobic patterns to prevent early bubble coalescence, and thus ensure the replenishment of liquid at the heating surface [21].

Surface wettability and the hydrophobic pattern effect on bubble departure behavior also affects the flow boiling heat transfer [22-24]. Kim et al. [24] experimentally explored the influence of heterogeneous wetting surfaces on flow boiling performance in a vertical macro-channel (D_h = 7.5 mm), in which wettability-patterned surfaces were combined with hydrophobic patterns (coated with Teflon; θ_c= 120°) and a hydrophilic surface (coated with SiO_2; θ_c= 57°). They found that the overall flow boiling heat transfer performance depended significantly on the design of the hydrophobic pattern and its corresponding dimensions and layout [24]; hydrophobic patterns with 1-mm inter-spacing, crossing or parallel to the flow direction, showed enhanced HTC and CHF compared to surfaces with 3-mm inter-spacing. They also suggested that the hydrophobic patterns should be able to break merged bubbles, with optimal sizing of the pattern resulting in a high HTC and CHF.

Additionally, in terms of homogeneous surfaces consisted of micro patterned arrays in flow boiling, Yin et al. [25] used an experimental method to investigated flow boiling heat

transfer on hybrid surfaces consisted of rough regions and inverted-triangle pin-fin arrays, which vertically aligned in the downstream region, under subcooled conditions. Their experimental results showed that the pressure drop induced in the channel significantly decreased as using the hybrid surfaces even in a relatively high flow rate and large heat flux regions. On the other hand, the overall flow boiling heat transfer performance can be further improved using heterogeneous surfaces, by combining both advantages of hydrophobic and hydrophilic surfaces (i.e., bubble nucleation can be promoted on hydrophobic islands and a premature dry-out can be suppressed using hydrophilic substrates).

As mentioned above, only a few studies have focused on the influence of wettability-patterned surfaces on flow boiling heat transfer characteristics. In particular, the effect of hydrophobic-patterned arrays with various shapes and inter-spacing under flow boiling conditions has still not been examined comprehensively. Hence, we manipulated the surface wettability to water, utilizing hydrophobic-patterned arrays and a hydrophilic substrate. Three hydrophobic patterns, i.e., circle, triangle, and inverted-triangle shapes, were created with variable inter-spacing, as shown in Fig. 1. The influence of the wettability-patterned surfaces on bubble detachment and flow boiling heat transfer characteristics, according to the shape and inter-spacing, was examined through heat transfer experiments and a bubble visualization method.

2. Experimental method

2.1 Experimental setup and procedure

In this study, we investigated the flow boiling heat transfer and bubble characteristics of various wettability-patterned surfaces. A schematic diagram of the experimental setup is shown in Fig. 2(a), consisting of four main components: (1) the working fluid-supply system, (2) the test section, (3) the heating system, and (4) the data acquisition system. The working fluid (deionized (DI) water, 18.2 MΩ/cm) was supplied via a constant temperature bath (Hanil Industrial Machine Co, Gwangju, Korea) with a capacity of 44 L. An immersion heater was used to maintain a working temperature of 100°C during the degassing procedure. The degassed fluid was stored in the main reservoir (i.e., a pressure valve was installed at the top of main reservoir to regulate the pressure conditions). A heat exchanger (Model 131001694) was used to regulate the fluid inlet temperature at 98.5±0.6°C, which was closed to the saturation temperature of DI water before pumping the saturated fluid into the test section. In

addition, the averaged fluid temperature at the inlet and outlet of the test section was treated as a bulk fluid temperature on the heated surface under saturated condition. A magnetic pump (TXS5.3, SUS316; Tuthil Co., Burr Ridge, IL, USA) with an electric motor (LG-OTIS, 3500rpm, Korea) continuously circulated the working fluid, resulting in a closed-loop system. The working fluid was maintained at a total mass flow rate of 0.51 kg/min, as monitored by a flowmeter (Ultra mass MK II, Tokyo, Japan) and an indicator (FC100P; FLOS Korea Co., Seoul, Korea). In addition, a test section with a rectangular channel, (i.e., the height and the width of channel are 5 mm, and D_h= 5 mm, respectively) was fabricated using polyetheretherketone with a low thermal conductivity (0.25 W/m-K), which was sufficient to achieve a fully developed flow (i.e., the entrance length L_e of the upstream region in the test section was longer than $4.4 \cdot Re^{1/6} \cdot D_h$). The Re was maintained at 6000 and the required length was 93.8mm. Two quartz windows were positioned on the side of the test section for observation of the wettability-patterned surfaces and bubble characteristics.

The heating system included a direct current power supply (300V-10A; KSC Korea Switching, Seoul, Korea). The power supply was connected to two copper bus bars located below the test plate, to heat the test surfaces according to different rated powers. A high-conductivity silver paste (resistivity: 10^{-4} Ω-cm) was spread uniformly over the interface between the copper bus bars and the heater electrodes to reduce contact resistance.

The data acquisition system consisted of K-type thermocouples (Omega Engineering, Stamford, CT, USA), a resistance temperature detector (RTD) sensor, an RTD signal module (SCXI-1503; National Instruments, Austin, TX, USA), and a data recorder (3490A; Agilent Technologies, Santa Clara, CA, USA). K-type thermocouples were utilized to measure the temperature of the working fluid at the inlet and outlet of the test section, and the RTD sensor was used to detect the surface temperature of the heating surfaces; both were connected to the data recorder and a personal computer to record and analyze temperature data under steady-state conditions. Figure 2(b) shows the RTD sensor configuration used to detect the surface temperature in the present study [26, 27]. The RTD sensor was made using a double-sided polished Si wafer created via a micro-electro mechanical system (MEMS) fabrication method, consisting of a silicon (Si) substrate with an insulation layer, five four-wire Pt circuits on the heating area for surface temperature measurements (5 mm × 10 mm), and a heater with two electrodes.

2.2 Wettability-patterned surfaces

The design of the various wettability-patterned surfaces is shown in detail in Fig. 3. Test surfaces were formed using a flat Si wafer, to negate surface roughness effects. The patterned surfaces were coated separately with a 200-nm-thick layer of SiO_2 and fluorooctyltrichlorosilane (FOTS) to form distinct wettability regions between the hydrophilic-coated surface and the hydrophobic pattern arrays. The apparent contact angle for the Si surface, the SiO_2-coated surface, and the FOTS-coated surface was 40°, 20°, and 110°, respectively, based on contact angle goniometer measurements (DSA100; Krüss, Hamburg, Germany), as shown in Fig. 3(a). The hydrophobic patterns were in the shape of a circle, triangle, and inverted triangle, with an inter-spacing of 0.75 and 1 mm, as shown in Fig. 3(b) and (c). The design information for the hydrophobic patterns is given in Table 1.

2.3 Droplet test and fabrication process on the wettability-patterned surfaces

The droplet test set-up for the wettability-patterned surfaces is shown in Fig. 4. We controlled the droplet volume at 5 μL by reference to the contact angle measurements, and took photographs with a microscope camera (U-CMAD3; Olympus, Tokyo, Japan) to determine the quality of the distinct wettability regions on the artificial surfaces. In the figure, the yellow and gray regions represent the FOTS hydrophobic-patterned arrays and SiO_2-coated substrates, respectively. The test results showed that the droplet covered the entire hydrophilic surface only, while the hydrophobic-coated surface remained mostly dry, thus indicating successful fabrication of the wettability-patterned test surfaces used in this study. Additionally, the detail information of the fabrication process of the wettability patterned surfaces is given in the supplementary materials.

2.4 Bubble characteristics on wettability patterned surfaces

Depending on the working conditions, the flow boiling heat transfer mechanism is strongly dependent on bubble characteristics, thus an appropriate analysis of bubble departure behavior can help the authors and readers to determine the cooling mechanisms of flow boiling by analyzing bubbles that form on heated surfaces. According to a previous work proposed by Kandlikar et al. [28], they suggested a criterion for classifying the categories of flow channels from convectional channels to molecular nanochannels depending on the hydraulic diameter of test chambers. For the bubble departure behavior in microchannels [29, 30], the bubble development process from bubble slug to the confined annular flow can be observed as well as the region of partial dry-out on heated surfaces from the top of flow channels as the heat flux

gradually elevated. On the other hand, the hydraulic diameter of the rectangular test section was 5 mm and the length of the main channel was 375 mm in the present work indicating that the test section was the convectional channel, which was relatively larger than those of the microchannel, resulting in different bubble characteristics on heated surfaces. Moreover, the bubble characteristics can be only observed at the sides of the test section and the heating area was designed in 5 mm in width and 10 mm in length, which was relatively small when compared with the test section, thus we only focused on bubble departure characteristics on heated surfaces such as bubble departure diameter and liquid paths instead of the confined flow patterns of bubbles due to the limitations of the experimental equipment.

In addition, the bubble detachment characteristics on heated surfaces were conducted on surfaces consisted of the hydrophilic substrate and the hydrophobic patterned arrays with various shapes using a high speed camera (Speedsense M310, Dantec, Denmar) with an 100W LED light source based on the shadowgraph method. All the required measurements regarding images of fully-detachment bubbles was analyzed by a commercial software (version 3.30, Dynamic Studio, Denmark) to determine the equivalent bubble departure diameter. By assuming that the measured 2D image of the bubble is a perfect circle, the software is able to analyze the equivalent diameter of fully-departing bubbles. The equation for the equivalent diameter of departing-bubbles is given by

$$d_b = 1.55 \cdot \frac{A_b^{0.625}}{p_b^{0.25}}$$

where A_b and P_b are the cross-sectional area and perimeter of the fully-detachment bubble, respectively [31].

2.5 Data reduction for boiling heat transfer characteristics

Parameters relevant to determine the CHF and HTC are discussed below. The heat transfer rate is defined as

$$q'' = \dot{Q}/A = \mathrm{I} \times \mathrm{V}/\mathrm{A} \quad (1)$$

where q'' is the heat transfer rate, A is the heated area, I is the input current, and V is the voltage imparted to the heater. Upon reaching the CHF, the local wall temperature increased sharply, by more than 20°C in 1 ms. The value of the CHF was calculated using the value halfway between the unstable heat flux obtained in the present study and a heat flux value obtained previously [26]. In this experiment, the wall temperature (T_w) was estimated using an

RTD sensor, which has five-points for measuring the surface temperature of the heating area. Each point of the RTD sensor was calibrated as follows:

$$T_{Rn} = b_n \times R_n + c_n \quad (2)$$

where T_{Rn} is the temperature of the RTD at sensor point n, R_n is the resistance of the sensor, and b_n and c_n are the calibration coefficients. The heating surface was on the top side of the RTD sensor, opposite the measurement points, and the thickness of the Si substrate was 500 μm. The conduction effect must be considered when evaluating the wall temperature based on Fourier's law for one-dimensional thermal conduction [32-34]:

$$q'' = k_{si}/l \times (T_R - T_w) \quad (3)$$

where k_{si} is the thermal conductivity of the Si substrate, l is the thickness of the RTD sensor, T_R is the temperature at the RTDs, and T_w is the wall temperature. To analyze the heat dissipation ability of the various wettability-patterned surfaces, we used Newton's law of cooling to evaluate the local HTC, which is expressed as follows:

$$q'' = h(T_w - T_f) \quad (4)$$

where h is the local HTC, T_w is the local wall temperature obtained from Eq. (3), and T_f is the bulk temperature of the working fluid, which corresponded to the average fluid temperature at the inlet and outlet of the flow channel.

2.6 Uncertainty analysis

The experimental uncertainties were estimated using the method proposed by Moffat [35]. The various uncertainties of the variables in this study are summarized in Table 2. According to the variation in the instruments and manual reading errors, the temperature of the working fluid based on the thermocouple readings and the dimensional error of the RTD sensor were ±0.2% and ±0.05%, respectively. Errors with respect to fluid properties were estimated based on the measured temperature. The propagation velocity of the working fluid was associated with an uncertainty in the Reynolds number (Re) of 4.6%. To evaluate the convective heat loss through the test surfaces, we used Fluent software (version 6.3.26; ANSYS, Canonsburg, PA, USA), a commercially available program for generating computational fluid dynamics code; here, we assumed that the heat spread area was the same as the area of convective heat transfer, which was estimated to be 6.3%. This convective heat loss was used to calculate the uncertainty

in the heat flux, including the CHF, given by

$$\left(\frac{\delta q''}{q''}\right) = \left[\left(\frac{\delta V}{V}\right)^2 + \left(\frac{\delta I}{I}\right)^2 + \left(\frac{\delta A}{A}\right)^2 + (q_{loss})^2\right]^{\frac{1}{2}} \quad (17)$$

where the imported voltage (V), current (I), and heating area (A) of the RTD sensor were used, and the calculated uncertainty of the heat flux was 6.3%. The uncertainty in the HTC is given by

$$\left(\frac{\delta h}{h}\right) = \left[\left(\frac{\delta q''}{q''}\right)^2 + \left(\frac{\delta T_w}{T_w}\right)^2 + \left(\frac{\delta T_f}{T_f}\right)^2\right]^{\frac{1}{2}} \quad (18)$$

Substituting the heat flux uncertainties, the investigated local wall temperature, and the temperature of the working fluid into Eq. (17), the uncertainty in the HTC was determined to be 9.0%.

The uncertainties in the local wall temperature measured by the RTD sensor, the heat flux, the HTC, and Re were 6.4%, 6.3%, 9.0%, and 4.6%, respectively. The pixel uncertainty in the bubble diameter that obtained from the bubble visualization was ±0.1 mm [36, 37].

3. Result and discussion

3.1 Flow boiling heat transfer on the wettability patterned surfaces

Figure 5(a) shows the temperature distribution of the wettability-patterned surfaces. Along the flow direction (i.e., from left to right), the surface temperature increased gradually in the upstream region from point 1 to point 4, and then decreased in the downstream region from point 4 to point 5, which can be attributed to bubble detachment behavior on the heating surface. Before vapor bubbles departed from the heating surface, bubble coalescence occurred more vigorously in the upstream region, resulting in an increasing trend in the surface temperature. The surface temperature decreased in the downstream region as the merged bubbles detached from the heating surface, thus indicating that when the heat flux reached CHF, only a specific region of the heating surface had reached the point of boiling crisis (i.e., a 20°C temperature spike was first observed markedly at point 4 of RTDs). In addition, the surface temperature distribution on test surfaces can be applicable to specific heat flux regions over ONB to CHF in this study.

Figure 5(b) shows the boiling characteristics of the various test surfaces, used to evaluate

the relationship between wall superheat and the relative heat flux given a Re value of 6,000. All wettability-patterned surfaces exhibited an enhancement in the CHF (243–255 W/cm^2), compared to the Si surface (178 W/cm^2), while the influences of inter-spacing and shape effects of the test surfaces with hydrophobic-patterned arrays on the CHF were insignificant.

In terms of the HTC of the test surfaces, Fig. 5(c) shows the relationship between the relative HTC and the heat flux for various wettability-patterned surfaces at point 4 of the RTD sensor for Re = 6,000. Surfaces consisted of hydrophobic-patterned arrays with a 1-mm inter-spacing and a hydrophilic substrate are represented by solid symbols; and the other heterogeneous-patterned surfaces with a 0.75-mm inter-spacing are represented by hollow symbols. Compared to the homogeneous Si-surface (represented by the red square symbol), the HTC of the wettability-patterned surfaces was superior (29.6–57.6 kw/m^2·K); this indicates that the surfaces consisted of hydrophobic-patterned array surface and hydrophilic substrate have a positive effect on flow boiling heat transfer.

Additionally, according to Fig. 6, the wettability-patterned surfaces showed an increasing trend in the HTC as the relative heat flux increased, when the hydrophobic-patterned shape was changed from circular to triangular; the trends were similar between the 0.75-mm and 1-mm inter-spacings. A surface with a fixed hydrophobic pattern showed enhancement in the HTC when the inter-spacing increased from 0.75 to 1 mm. Thus, it can be conjectured that the difference in flow boiling heat transfer among all of the artificial surfaces in this study was predominantly due to the relative inter-spacing between neighboring patterns and the shape of the hydrophobic-patterned arrays.

3.2 Bubble characteristics on the wettability patterned surfaces

Figure 7(a) and (b) show the bubble detachment characteristics on the wettability-patterned surfaces, in terms of the bubble departure diameter and the bubble detachment frequency according to the relative heat flux. Compared to the Si-surface, the surface consisting of triangle-shaped hydrophobic-patterned arrays and a hydrophilic substrate showed the smallest bubble diameter and the highest bubble detachment frequency, which is in agreement with the relationship between the bubble lift force acting on the various hydrophobic patterns and the flow boiling heat transfer. The inter-spacing effect of the wettability-patterned surfaces on bubble characteristics can also be observed by comparing test surfaces with the same hydrophobic shape. The bubble departure diameter increased as the inter-spacing between hydrophobic patterns narrowed, which in turn reduced the bubble release frequency. As mentioned above, the flow boiling heat transfer characteristics are dominated by both the shape

of the hydrophobic patterned arrays and the inter-spacing between neighboring patterns.

The bubble departure behavior was difficult to observe in the high heat flux region via the visualization method used herein, owing to vapor bubbles merging readily as the heat flux rose and being affected by the shear lift force of the working fluid, especially downstream of the heating surface. Hence, bubble visualization results were recorded in the analytical upstream region along the flow direction for all test surfaces, as shown in Fig. 7(c); the fixed region was 2 mm in length and 1.5 mm in width.

We selected the triangle-shaped hydrophobic-patterned surface with 1-mm inter-spacing as a representative case for comparison with the homogeneous Si-surface when the heat flux was 80 W/cm^2, as this surface demonstrated the highest overall flow boiling heat transfer performance, according to Fig. 8(a). The bubble visualization results showed that vapor bubbles that formed on the wettability-patterned surface maintained more of the liquid path compared to the Si-surface, allowing more cooling liquid to reach the heating surface. In contrast, if the heat flux increased in a specific high heat flux region (before reaching the CHF), the bubble characteristics on the wettability-patterned surface were more difficult to resolve, owing to irregular bubbles that merged and moved along the heating surface. Thus, bubble behavior on the test surfaces was difficult to characterize directly. Nevertheless, Sun et al [20] experimentally demonstrated the effectiveness of Teflon hydrophobic-patterned arrays on wettability-patterned surfaces in enhancing boiling heat transfer. For a heat flux of 206 W/cm^2, bubble nucleation sites on the hydrophobic surfaces were still observed via bubble visualization, even in the high heat flux region, under sub-cooling conditions. However, several bubble nucleation sites formed on the wettability-patterned surface consisting of triangle-shaped hydrophobic-patterned arrays, whereas the entire heating surface of the Si-surface was continuously covered by merged bubbles when the heat flux was raised to 170 W/cm^2, as shown in Fig. 8(b). These results indicate that the shape effect of the hydrophobic patterns can be optimized to improve flow boiling heat transfer, even in the high heat flux regime.

3.3 Temporal surface temperature of the wettability-patterned surface at CHF

Figure 9 shows the temporal surface temperature at points 1–5 of the RTD sensor for the test surfaces, which included the Si surface and the 1-mm inter-spacing wettability-patterned surfaces with a circular hydrophobic pattern, an inverted triangle-shaped hydrophobic pattern, and a triangle-shaped hydrophobic pattern when the heat flux was at the CHF. Standard deviations were considered in the analysis of temperature variation; the temperature varied over time at point 4 of the RTD sensor for all of the representative test cases. The surface with the

triangle-shaped hydrophobic-patterned arrays showed the lowest standard deviation, of 1.55 K, among all patterns; this indicates that the shape effect of the hydrophobic pattern affects the bubble detachment characteristics, even in the high heat flux regime, where some hydrophobic patterns can release vapor bubbles more efficiently. The results regarding temporal surface temperature were in agreement with the discussion above regarding the bubble visualization results for all of the test surfaces.

3.4 Influence of spacing between neighboring hydrophobic patterns on bubble nucleation

We hypothesized that the influence of thermal interactions would become stronger when the inter-spacing between neighboring hydrophobic patterns decreased. This is in agreement the findings of Sujith et al. [21], where the promotive effect of bubble nucleation on adjacent nucleation sites existed only if the inter-distance between two neighboring hydrophobic patterns was sufficiently small; specifically, when bubble coalescence occurs prematurely, the contact line of a merged bubble will move towards the hydrophilic substrate, thereby inhibiting the recirculation of liquid to the heating surface. Figure 10 compares the present results to the experimental data of Nimkar et al. [17], which were obtained under similar conditions, using the empirical correlation proposed by Calka et al. [38]. The test surfaces in this study consisted of circular hydrophobic-patterned arrays and a hydrophilic substrate, with 0.75- and 1-mm inter-spacings selected as representative cases. The shape parameter is defined as the ratio of the radius of the liquid microlayer underneath the bubble which corresponds to the radius of the bubble contact line (R_b) and the actual bubble radius (R_m), according to Zhang et al. [39]. The surface with re-entrant pyramidal cavities and 0.5-mm inter-spacing, which showed the lowest heat dissipation capacity under pool boiling conditions, was located deep within the repulsive region, compared to the surfaces with 0.75- and 1-mm inter-spacing. Thus, the narrow inter-spacing between two adjacent nucleation sites inhibited bubble nucleation, leading to a deterioration in the overall boiling heat transfer performance.

Additionally, the present experiment empirically assessed the correlation region for $S/D_d > 3$, which represents the region of no interaction between bubble nucleation; this is due to the effect of the shear lift force of the working fluid on bubble formation, which results in a relatively small mean bubble diameter and a shift to the right of the value of the non-dimensional separation distance. ~~Hence, the experimental results for the wettability-patterned surfaces were not within the valid range.~~ The influence of the inter-spacing of the heterogeneous hydrophobic-patterned surfaces on forced convective boiling can be explained by reference to the work of Baltic et al. [40], who showed that the frequency of bubble

nucleation on the downstream hydrophobic pattern is lower when vapor bubbles start to form on the upstream hydrophobic pattern. Thus, when thermal interaction occurs between neighboring nucleation sites, the inhibitory effect of bubble nucleation becomes more significant as the inter-spacing decreases.

Notably, the influence of wettability patterned shapes also plays an important role on flow boiling heat transfer, which will be discussed in the next section.

3.5 Shape effect and bubble lift force of the hydrophobic-patterned arrays on flow boiling heat transfer

Figure 11(a) shows that when the inter-spacing between adjacent hydrophobic patterns is 0.75 mm, the hydrophobic-patterned arrays with a triangle shape showed heat transfer capacity that was 47% and 16% higher, respectively, than that of surfaces with circular and inverted triangle shapes. Interestingly, a similar enhancement in flow boiling heat transfer also was evident in the wettability-patterned surfaces with 1-mm inter-spacing, as shown in Fig. 11(b); this indicates that the various hydrophobic patterns affect flow boiling heat transfer as the wall superheat increases.

To determine the influence of the shape of the various hydrophobic patterned surfaces on flow boiling heat transfer characteristics, it is important to understand the relationship between the surface tension forces of individual bubbles and the hydrophobic-patterned shapes that act on bubble behavior. In flow boiling, the vapor bubbles usually slide along the heating surface and subsequently lift off at some distance downstream in the flow channel; the mean bubble diameter at departure depends significantly on the mean liquid velocity, as well as the wall superheat. Figure 12 depicts the force balance between bubbles and the hydrophobic pattern in a horizontal channel. The forces acting on the bubble can be divided into two separate components in the *x*-direction and the *y*-direction. If the surface tension force in the *x*-direction (F_{sx}), which is opposite to the shear lift force of the working fluid, becomes relatively small, the bubble will start to slide along the heating surface. In contrast, when the surface tension force in the *y*-direction (F_{sy}), which is opposite to the buoyant force, becomes small, the bubble that forms on the hydrophobic pattern will lift off more easily. In addition, the polar angle (φ) of the hydrophobic patterns, the bubble dynamic contact angles (α and β), and the bubble contact line (d_w) on the hydrophobic patterns are key parameters for estimating the relative surface tension force in the *x* and *y* directions. The bubble dynamic contact angles can be differentiated as the advancing contact angle (α) and the receding contact angle (β); these angles can be difficult to measure accurately, as bubble formation is strongly affected by the shear lift force of the working fluid. Therefore, in this study, we assumed that the bubble

dynamic contact angles α and β were 50° and 40°, respectively for the hydrophobic patterns having circle, triangle, and inverted triangle shapes. The basis of the assumption of bubble dynamic contact angles is given in the supplementary material.

Figure 13 shows the direction of surface tension forces on the various hydrophobic patterns according to the concept of polar coordinates, which depends on the shape of the pattern along the flow direction. For the circular hydrophobic pattern, the definitions of the surface tension force in the *x* and *z* directions are the same as those defined in previous work on bubble force balance under forced convective boiling [41]. In contrast, the components of the surface tension force acting on the hypotenuse of the triangle-shaped hydrophobic pattern are identical to the forces acting on the inverted triangle shape, but differ on the base side. In terms of the triangle shape, the surface tension force acting on the base side is dominated by the advancing contact angle (α) along the flow direction; whereas the surface tension force acting on the base side of the inverted triangle is dominated by the receding contact angle (β), which is opposite to the flow direction, as shown in Figs. 13(b) and (c).

It is widely known that boiling heat transfer characteristics are dominated by the bubble detachment behavior on the heating surface, with better boiling heat transfer performance being observed when the bubble departure frequency increases. As such, we used the expressions proposed by Klausner et al. [41] for describing surface tension forces to mathematically analyze the relationship between bubble detachment and flow boiling heat transfer characteristics. Before calculating the components of the surface tension force in the *x* and *y* directions, we must distinguish the advancing contact angle (α) from the receding contact angle (β) on the various wettability-patterned surfaces. In this experiment, we combined both contact angles (α and β) into a general contact angle (γ) to calculate the surface tension forces. However, the definition of the bubble dynamic contact angle for test surfaces with a circular hydrophobic-patterned array is the same as that defined in the study by Klausner et al. [41]. Accordingly, a third-order polynomial is assumed for the general contact angle (γ) on the surface, giving the following expression for the triangle hydrophobic-patterned array:

$$\gamma_1(r) = \frac{(\alpha-\beta)}{L} r_1 + \beta \ , \ r_1 \approx a\sim 0 \tag{5}$$

$$\gamma_2(r) = \alpha \ , \ \varphi_2 = -\frac{\pi}{6} \tag{6}$$

where γ_1 is the general contact angle on the hypotenuse of the triangle pattern, γ_2 is the general

contact angle on the base side of the triangle pattern, α is the advancing contact angle, β is the receding contact angle, φ_2 is the polar angle around the bubble, L is the absolute length of the triangle pattern, and r_1 is the distance from point a to the original point 0 along the flow direction, which satisfies $\gamma_1(L) = \alpha$, $\gamma_1(0) = \beta$ and the symmetry conditions $\gamma_1'(0) = \gamma_1'(L) = 0$. The relative components of the surface tension force on the triangle hydrophobic pattern in the *x* and *y* directions are expressed as follows:

$$F_{sx} = \sigma \int_a^0 cos\gamma_1 \cdot cos\varphi_2 \cdot dr - \sigma \int_0^{-\frac{\pi}{6}} r cos\gamma_2 \cdot cos\varphi_2 \cdot d\varphi \quad (7)$$

$$F_{sy} = -\int_0^{-\frac{\pi}{6}} r \cdot \sigma \cdot sin\gamma d\varphi \quad (8)$$

where F_{sx} is the surface tension force in the *x*-direction, F_{sy} is the surface tension force in the *y*-direction, and σ is the surface tension of the working liquid under saturated conditions. Substituting Eqs. (5) and (6) into Eqs. (7) and (8), respectively, the intergradient results are given by

$$F_{sx} = \frac{\sqrt{3}}{2}\sigma L\left[\frac{(sin\beta - sin\alpha)}{\alpha - \beta} - \frac{\pi}{6}\cos\alpha\right] \quad (9)$$

$$F_{sy} \cong -0.4757\sigma L \sin\alpha \quad (10)$$

In addition, the third-order polynomials assumed for the general contact angle (γ) for the surface with an inverted triangle-hydrophobic shape are defined as follows:

$$\gamma_3(r) = \frac{(\beta - \alpha)}{L} r_2 + \alpha \ , \ r_2 \approx 0 \sim a \quad (11)$$

$$\gamma_4(r) = \beta \ , \ \varphi_3 = \frac{\pi}{6} \quad (12)$$

where γ_3 is the general contact angle on the hypotenuse of the inverted triangle pattern, γ_4 is the general contact angle on the base side of the inverted triangle pattern, φ_3 is the polar angle around the bubble, *L* is the absolute length of the inverted triangle pattern, and r_2 is the distance from the original point 0 to point *a* in the flow direction. The relative components of the surface tension force in the *x* and *y* directions can be expressed, as follows:

$$F_{sx} = \sigma \int_0^a cos\gamma_3 \cdot cos\varphi_3 \cdot dr + \sigma \int_0^{\frac{\pi}{6}} r cos\gamma_4 \cdot cos\varphi_3 \cdot d\varphi \quad (13)$$

$$F_{sy} = -\int_0^{\frac{\pi}{6}} r \cdot \sigma \cdot sin\gamma d\varphi \quad (14)$$

Substituting Eqs. (11) and (12) into Eqs. (13) and (14), respectively, the inter-gradient results are given by

$$F_{sx} = \frac{\sqrt{3}}{2}\sigma L\left[\frac{(sin\beta - sin\alpha)}{\beta - \alpha} + \frac{\pi}{6}\cos\alpha\right] \quad (15)$$

$$F_{sy} \cong -0.4757\sigma L\, sin\,\beta \quad (16)$$

In this experiment, the advancing contact angle (α) and receding contact angle (β) were assumed to be 50° and 40°, respectively. With respect to the different shapes of hydrophobic-patterned arrays, the diameter of the circular shape was 0.15 mm, and the length of the triangle and the inverted triangle shapes were 0.201 mm. Considering that bubble behavior is affected by the surface tension forces in the *x* and *y* directions, we used the force ratio of F_{sy} to F_{sx} to represent the lift force acting on bubbles that form on the patterned surfaces, to analyze the influence of bubble detachment characteristics on the overall flow boiling heat transfer performance. The force ratio (F_{sy}/F_{sx}) for the wettability-patterned surfaces with circular, inverted triangle, and triangle hydrophobic-patterned arrays were 0.06, 0.85, and 1.21, respectively, which agrees with the experimental results regarding the relative HTC for all wettability-patterned surfaces in this study, as shown in Fig. 14.

The comparison of the wettability-patterned surfaces with respect to the bubble lift force acting on the hydrophobic patterns and the relative HTC demonstrates that the overall flow boiling heat transfer performance is dominated by the shape of the hydrophobic pattern and the inter-spacing between neighboring patterns on the hydrophilic substrate. However, the surfaces with triangular hydrophobic-patterned arrays show a larger bubble lift force compared to the circular and inverted triangle shapes. Thus, vapor bubbles can be removed more efficiently from the triangle-patterned surface, and the hydrophobic-patterned array with a triangle shape was the optimal design among the wettability-patterned surfaces in the present study.

4. Conclusions

This experimental study examined the flow boiling heat transfer characteristics of wettability-patterned surfaces with hydrophobic-patterned arrays in the shape of a circle, triangle, and inverted triangle. The inter-spacing between neighboring nucleation sites were 0.75 mm and 1 mm, and the mass flow rate was fixed at 0.51 kg/min (i.e., Re = 6,000) at atmospheric pressure. Our results are summarized below.

1. The surface with hydrophobic-patterned arrays showed enhanced flow boiling heat transfer characteristics, in terms of the CHF (40–43%) and HTC (35–163%), compared to a homogeneous Si-surface.
2. In terms of the shape effect of hydrophobic-patterned arrays, the surface with a triangle hydrophobic-patterned array showed a higher heat dispassion capacity than the surfaces with hydrophobic patterns that consisted of circle and inverted-triangle shapes, by 47% and 16%, respectively. In addition, bubbles that formed on the wettability-patterned surfaces were released more efficiently than those on the Si-surface, owing to the difference in bubble lift forces and consequently smaller bubble departure diameter. The bubble size depended on the shape of the hydrophobic-patterned array.
3. When the shape of the hydrophobic patterns was fixed, narrowing of the inter-spacing between the two adjacent patterns (i.e., from 1 to 0.75 mm) resulted in stronger thermal interactions, which inhibited bubble nucleation on the wettability-patterned surfaces and subsequently deteriorated the overall flow boiling heat transfer performance.
4. Several bubble nucleation sites were observed on the wettability-patterned surfaces when the heat flux was at 170 W/cm^2. The standard deviation of the temporal surface temperature for the test surfaces consisting of the hydrophobic-patterned arrays and a hydrophilic substrate were much smaller than that of the Si-surface, indicating that the hydrophobic patterns affected the flow boiling heat transfer characteristics, even in the high heat flux region.
5. This study examined the influence of hydrophobic-patterned arrays on bubble detachment characteristics by analyzing the bubble lift force acting on the hydrophobic-patterned arrays in the flow direction. The experimental results are relevant to flow boiling heat transfer and could be used to optimize the design of heterogeneous wettability-patterned surfaces.

Acknowledgement

This work was supported by the Human Resources Development program (No.20204030200110) of the Korea Institute of Energy Technology Evaluation and Planning(KETEP) grant funded by the Korea government Ministry of Trade, Industry and Energy.

Declaration of Competing Interest

The authors declare no competing financial interest.

REFERENCES

[1] Phan, H. T., Caney, N., Marty, P., Colasson, S. & Gavillet, J. Surface wettability control by nanocoating: The effects on pool boiling heat transfer and nucleation mechanism. International Journal of Heat and Mass Transfer, 52 (2009), 5459–5471.

[2] Hui Zhang, Mudawar, I. & Hasan, M. M. Application of Flow Boiling for Thermal Management of Electronics in Microgravity and Reduced-Gravity Space Systems. IEEE Transactions on Components and Packaging Technologies 32 (2009), 466–477.

[3] Suzuki, K., Yuki, K. & Mochizuki, M. Application of Boiling Heat Transfer to High-Heat-Flux Cooling Technology in Power Electronics. Transactions of The Japan Institute of Electronics Packaging 4 (2011), 127–133.

[4] Karayiannis, T. G. & Mahmoud, M. M. Flow boiling in microchannels: Fundamentals and applications. Applied Thermal Engineering 115 (2017), 1372–1397.

[5] Jo, H., Ahn, H. S., Kang, S. & Kim, M. H. A study of nucleate boiling heat transfer on hydrophilic, hydrophobic and heterogeneous wetting surfaces. International Journal of Heat and Mass Transfer 54 (2011), 5643–5652.

[6] Sur, A., Lu, Y., Pascente, C., Ruchhoeft, P. & Liu, D. Pool boiling heat transfer enhancement with electrowetting. International Journal of Heat and Mass Transfer 120 (2018), 202–217.

[7] Kim, J. M. et al. Smart surface in flow boiling: Spontaneous change of wettability. International Journal of Heat and Mass Transfer 105 (2017), 147–156.

[8] Yim, K., Lee, J., Naccarato, B. & Kim, K. J. Surface wettability effect on nucleate pool boiling heat transfer with titanium oxide (TiO2) coated heating surface. International Journal of Heat and Mass Transfer 133 (2019), 352–358.

[9] Betz, A. R., Xu, J., Qiu, H. & Attinger, D. Do surfaces with mixed hydrophilic and hydrophobic areas enhance pool boiling? Appl. Phys. Lett. 97 (2010), 141909.

[10] Betz, A. R., Jenkins, J., Kim, C.-J. 'CJ' & Attinger, D. Boiling Heat Transfer on Superhydrophilic, Superhydrophobic, and Superbiphilic Surfaces. International Journal of Heat and Mass Transfer 57 (2013), 733–741.

[11] Takata, Y., Hidaka, S. & Kohno, M. Effect of surface wettability on pool boiling: enhancement by hydrophobic coating. Int. J. Air-Cond. Ref. 20 (2012), 1150003.

[12] Coyle, C., O'Hanley, H., Phillips, B., Buongiorno, J. & McKrell, T. Effects of Hydrophobic Surface Patterning on Boiling Heat Transfer and Critical Heat Flux of Water at Atmospheric Pressure. ASME (2013).

[13] Wang, X., Zhao, S., Wang, H. & Pan, T. Bubble formation on superhydrophobic-micropatterned copper surfaces. Applied Thermal Engineering 35 (2012), 112–119.

[14] Shen, B. et al. Bubble activation from a hydrophobic spot at "negative" surface superheats in subcooled boiling. Applied Thermal Engineering 88 (2015), 230–236.

[15] Wi, Y. et al. Optimal Patterned Wettability for Microchannel Flow Boiling Using the Lattice Boltzmann Method. Coatings 8 (2018), 288.

[16] Goel, P., Nayak, A. K., Ghosh, P. & Joshi, J. B. Experimental study of bubble departure characteristics in forced convective subcooled nucleate boiling. Experimental Heat Transfer 31 (2018), 194–218.

[17] Nimkar, N. D., Bhavnani, S. H. & Jaeger, R. C. Effect of nucleation site spacing on the pool boiling characteristics of a structured surface. International Journal of Heat and Mass Transfer 49 (2006), 2829–2839.

[18] Jo, H., Kim, S., Park, H. S. & Kim, M. H. Critical heat flux and nucleate boiling on several heterogeneous wetting surfaces: Controlled hydrophobic patterns on a hydrophilic substrate. International Journal of Multiphase Flow 62 (2014), 101–109.

[19] Choi, C.-H. et al. Large-scale Generation of Patterned Bubble Arrays on Printed Bi-functional Boiling Surfaces. Scientific Reports 6 (2016), 23760.

[20] Sun, Z., Chen, X. & Qiu, H. Bubble Dynamics and Heat Transfer During Pool Boiling on Wettability Patterned Surfaces. Heat Transfer Engineering 39 (2018), 663–671.

[21] Sujith, C. V. S. et al. Experimental Investigation on the Effect of Size and Pitch of Hydrophobic Square Patterns on the Pool Boiling Heat Transfer Performance of Cylindrical Copper Surface. in (2018).

[22] Zhu, Y. et al. Surface Structure Enhanced Microchannel Flow Boiling. J. Heat Transfer 138 (2016), 091501.

[23] Wang, H., He, M. & Qiu, H. Bubble Dynamics and Flow Boiling Characteristics in a Chemically Patterned Microchannel. in (2018).

[24] Kim, J. M. et al. Effect of heterogeneous wetting surface characteristics on flow boiling performance. International Journal of Heat and Fluid Flow 70 (2018), 141–151.

[25] Yin, L., Chauhan, A., Recinella, A., Jia, L. & Kandlikar, S. G. Subcooled flow boiling in an expanding microgap with a hybrid microstructured surface. International Journal of Heat and Mass Transfer 151 (2020), 119379.

[26] Shin, S. et al. Enhanced Boiling Heat Transfer using Self-Actuated Nanobimorphs. Nano Letters 18 (2018), 6392–6396.

[27] Shin, S., Choi, G., Kim, B. S. & Cho, H. H. Flow boiling heat transfer on nanowire-coated surfaces with highly wetting liquid. Energy 76 (2014), 428–435.

[28] Kandlikar, S. G. & Grande, W. J. Evolution of Microchannel Flow Passages–Thermohydraulic Performance and Fabrication Technology. Heat Transfer Engineering 24 (2003), 3–17.

[29] Li, W., Zhou, K., Li, J., Feng, Z. & Zhu, H. Effects of heat flux, mass flux and two-phase inlet quality on flow boiling in a vertical superhydrophilic microchannel. International Journal of Heat and Mass Transfer 119 (2018), 601–613.

[30] Li, W., Luo, Y., Zhang, J. & Minkowycz, W. J. Simulation of Single Bubble Evaporation in a Microchannel in Zero Gravity with Thermocapillary Effect. J. Heat Transfer 140 (2018).

[31] Koch P, Equivalent diameters of rectangular and oval ducts, Build Serv. Eng. Res. Technol. 29 (2008),341-347.

[32] Kim, B. S. et al. Stable and uniform heat dissipation by nucleate-catalytic nanowires for boiling heat transfer. International Journal of Heat and Mass Transfer 70 (2014), 23–32.

[33] Choi, G., Shim, D. I., Lee, D., Kim, B. S. & Cho, H. H. Enhanced nucleate boiling using a reduced graphene oxide-coated micropillar. International Communications in Heat and Mass Transfer 109 (2019), 104331.

[34] Lee, D., Lee, N., Hsu, W.-T., Yun, M. & Cho, H. H. Enhanced boiling heat transfer on micro-structured surfaces via ultrasonic actuation. International Communications in Heat and Mass Transfer 113 (2020), 104512.

[35] R.J. Moffat, Contributions to the theory of single-sample uncertainty analysis, ASME J. Fluids Eng. 104 (1982), 250–258.

[36] Peyghambarzadeh, S. M., Hatami, A., Ebrahimi, A. & Fazel, A. Photographic study of bubble departure diameter in saturated pool boiling to electrolyte solutions. Chemical Industry and Chemical Engineering Quarterly 20, 143–153 (2014).

[37] Lee, D., Lee, N., Shim, D. I., Kim, B. S. & Cho, H. H. Enhancing thermal stability and uniformity in boiling heat transfer using micro-nano hybrid surfaces (MNHS). Applied Thermal Engineering 130 (2018), 710–721.

[38] Calka, A. & Judd, R. L. Some aspects of the interaction among nucleation sites during saturated nucleate boiling. International Journal of Heat and Mass Transfer 28 (1985), 2331–2342.

[39] Zhang, L. & Shoji, M. Nucleation site interaction in pool boiling on the artificial surface. International Journal of Heat and Mass Transfer 46 (2003), 513–522.

[40] Baltis, C. & van der Geld, C. Experimental investigation of the thermal interactions of nucleation sites in flow boiling. International Journal of Heat and Mass Transfer 78 (2014), 1208–1218.

[41] Klausner, J. F., Mei, R., Bernhard, D. M. & Zeng, L. Z. Vapor bubble departure in forced convection boiling. International Journal of Heat and Mass Transfer 36 (1993), 651–662.

Table Captions

Table 1 Details of the hydrophobic coating pattern design

Table 2 Experimental measurement uncertainties

Table 1 Details of the hydrophobic coating pattern design

Test surfaces	Structure	Diameter/ Length [mm]	Inter-spacing [mm]	Number
S1	Circle	0.15	0.75	98
S2	Circle	0.15	1	50
S3	Triangle	0.201	0.75	98
S4	Triangle	0.201	1	50
S5	Inverted triangle	0.201	0.75	98
S6	Inverted triangle	0.201	1	50

Table 2 Experimental measurement uncertainties

Parameter	Uncertainty
Temperature measurement [℃]	0.2℃
Heater power measurement	6.3%
q_{loss}	6.3%
T_s	6.4%
L	0.2%
μ, ρ	1.5%
V_f	3.9%
Re	4.6%
h	9.0%

Figure Captions

Figure 1 Schematic diagram showing the effects of surface wettability and hydrophobic pattern, which include shape and inter-spacing effects, on the overall flow boiling heat transfer.

Figure 2 Experimental setup. (a) Flow boiling experimental apparatus. (b) Resistance temperature detector (RTD) sensor.

Figure 3 Schematic diagram of various wettability-patterned surfaces. (a) Wettability of the hydrophobic and hydrophilic surfaces. (b) Configurations of wettability-patterned surfaces. (c) Detailed design of the different patterned surfaces (circle, triangle, and inverted triangle).

Figure 4 Annotated photograph and droplet test of wettability-patterned surfaces.

Figure 5 (a) Surface temperature distribution over the local sensor points of the RTD sensor. (b) Relationship between wall superheat and relative heat flux for various wettability-patterned surfaces. (c) Heat flux versus the heat transfer coefficient (HTC) for various patterned surfaces at point 4 of the RTD sensor (Reynolds number, Re: 6,000).

Figure 6 Comparison of the HTC between the wettability-patterned surfaces and the Si surface.

Figure 7 Bubble detachment characteristics for the wettability-patterned surfaces at Re = 6,000. Relationship between (a) the bubble departure diameter and the relative heat flux and (b) the bubble departure frequency and the relative heat flux. (c) Analytic region of upstream bubble characteristics along the flow direction.

Figure 8 Bubble detachment from the wettability-patterned surfaces with 1-mm spacing with heat flux of (a) 80 and (b) 170 W/cm^2.

Figure 9 Temporal surface temperature for wettability-patterned surfaces with 1-mm spacing at various points of the RTD sensor: (a) Si surface and hydrophobic-patterned surfaces having a (b) circle, (c) inverted triangle, and (d) triangle pattern.

Figure 10 Relationship between the shape parameter and the non-dimensional separation distance for various wettability-patterned surfaces.

Figure 11 Relationship between wall superheat and the relative heat flux for various wettability-patterned surfaces at Re = 6,000. Patterned surfaces with a (a) 0.75-mm and (b) 1.0-mm inter-spacing.

Figure 12 Schematic diagram of the bubble lift force acting on a single hydrophobic pattern in a horizontal conventional channel.

Figure 13 Schematic diagram of the shape effect of hydrophobic patterns on bubble lift force in the flow direction: (a) circle, (b) triangle, and (c) inverted triangle hydrophobic patterns.

Figure 14 Relationship between the bubble lift force and the HTC for the wettability-patterned surfaces (Re = 6,000).

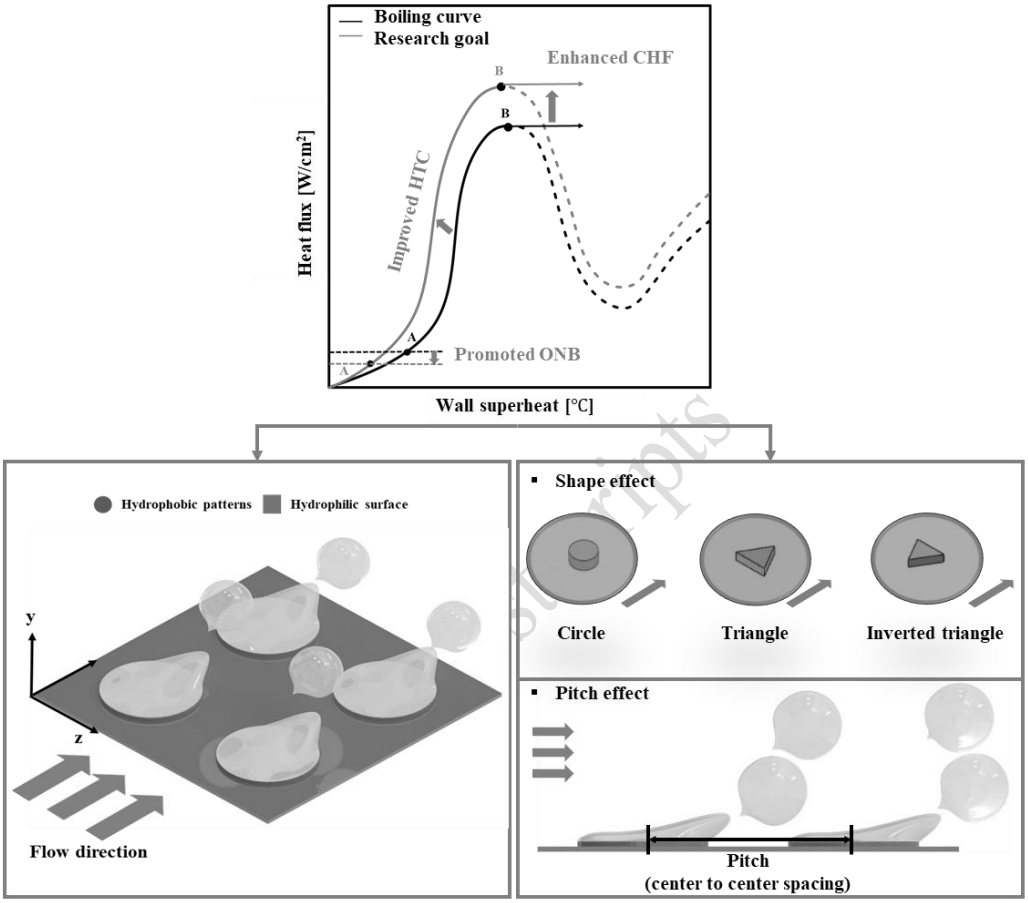

Figure 1 Schematic diagram showing the effects of surface wettability and hydrophobic pattern, which include shape and inter-spacing effects, on the overall flow boiling heat transfer.

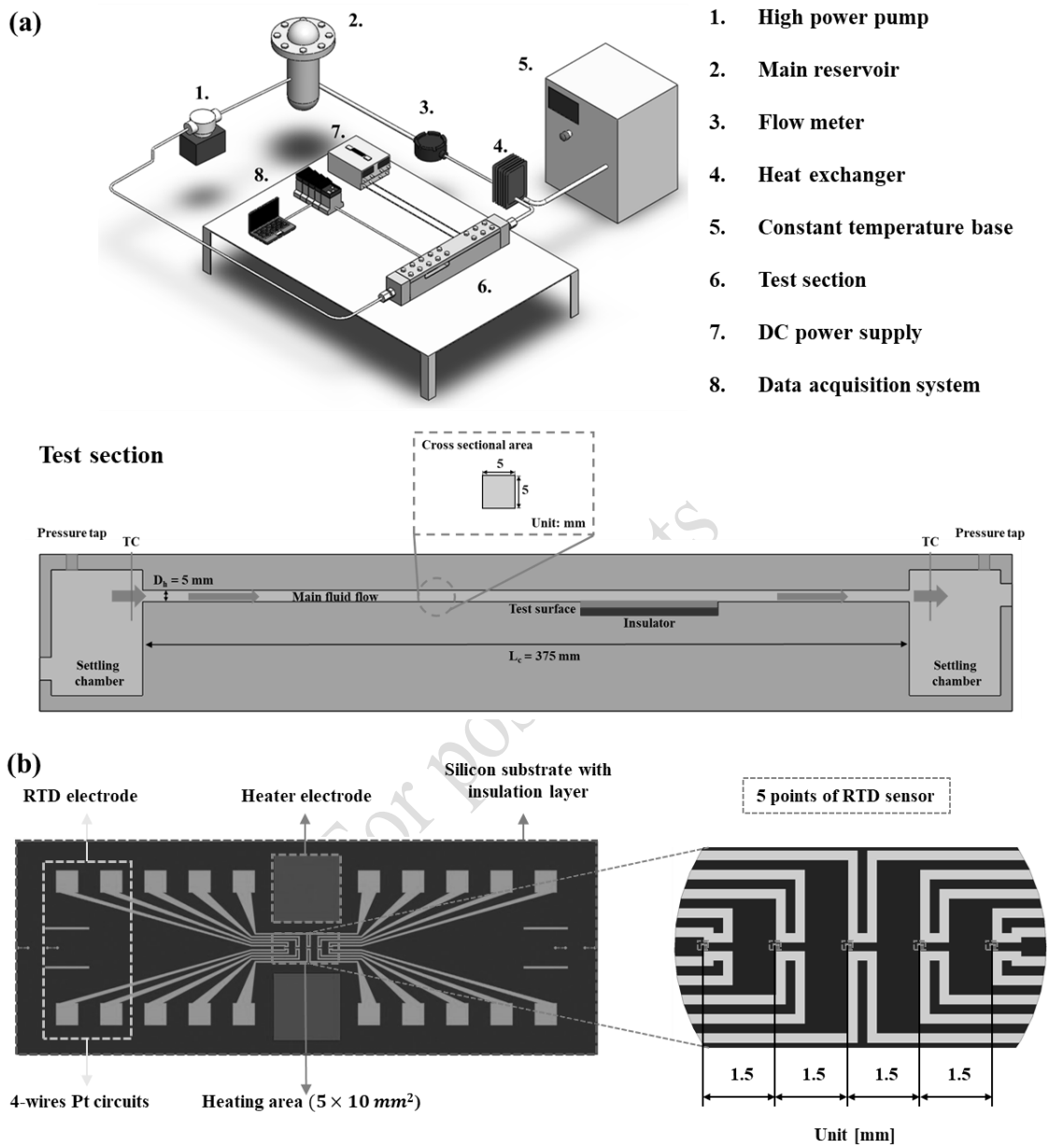

Figure 2 Experimental setup. (a) Flow boiling experimental apparatus. (b) Resistance temperature detector (RTD) sensor [26, 27].

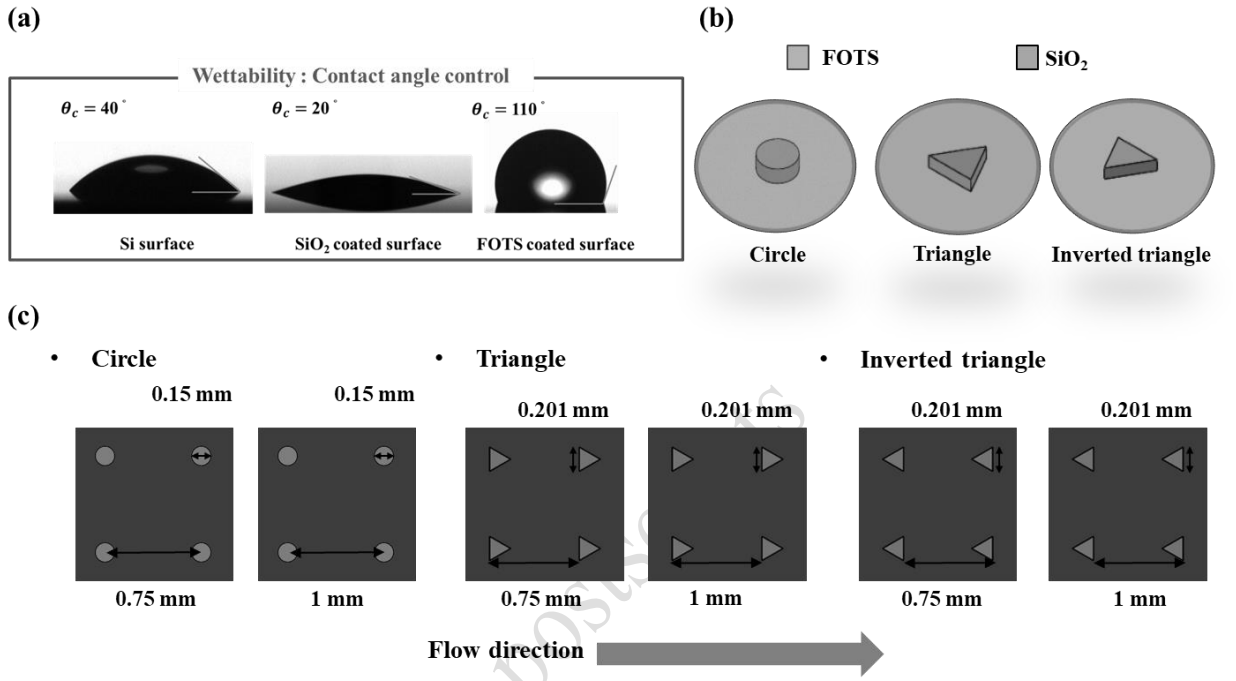

Figure 3 Schematic diagram of various wettability-patterned surfaces. (a) Wettability of the hydrophobic and hydrophilic surfaces. (b) Configurations of wettability-patterned surfaces. (c) Detailed design of the different patterned surfaces (circle, triangle, and inverted triangle).

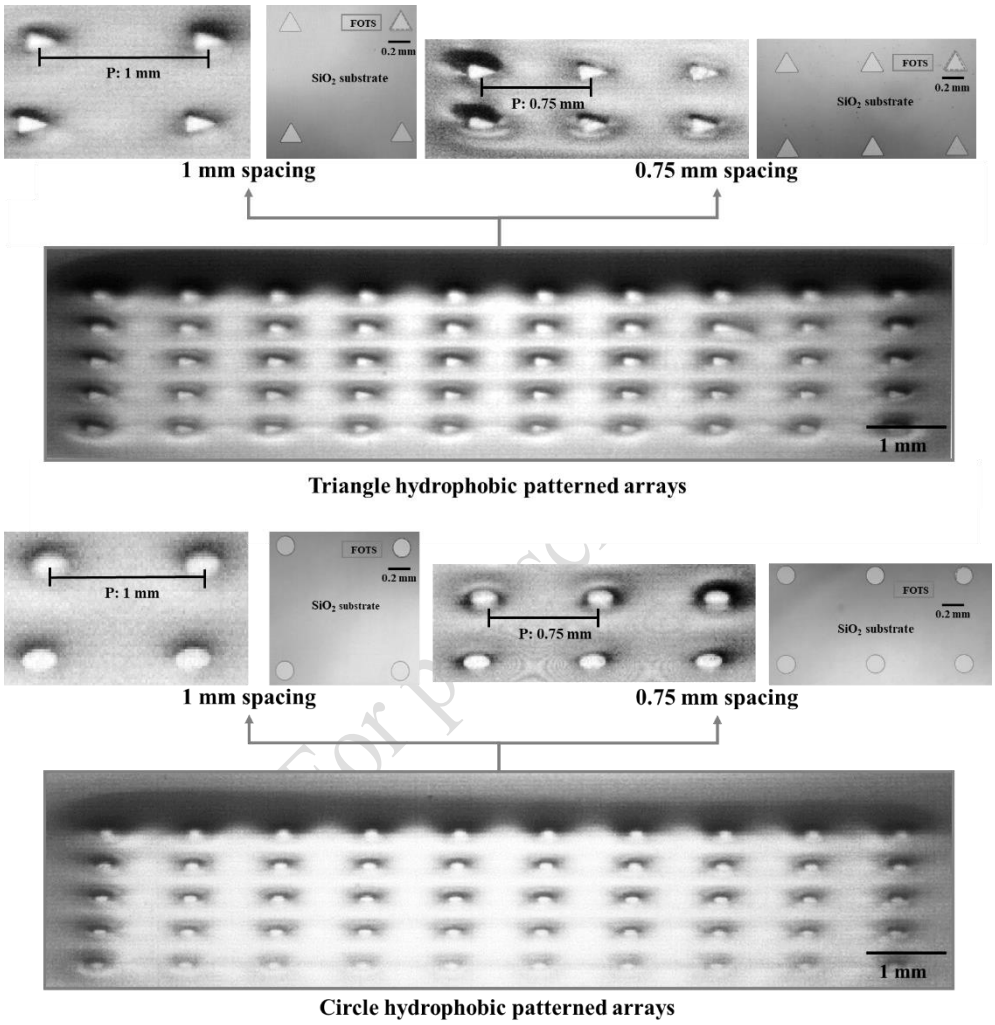

Figure 4 Annotated photograph and droplet test of wettability-patterned surfaces.

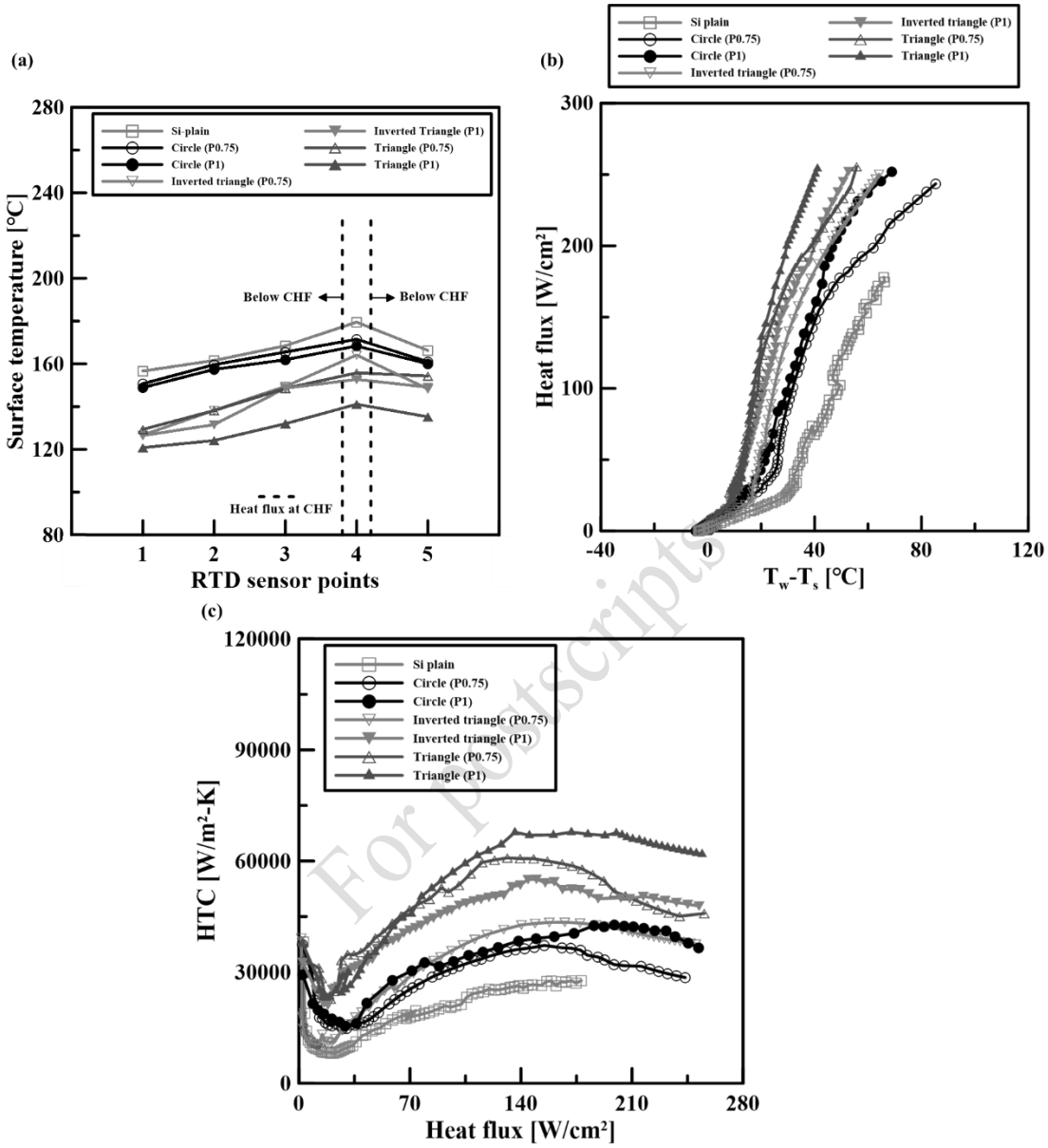

Figure 5 (a) Surface temperature distribution over the local sensor points of the RTD sensor. (b) Relationship between wall superheat and relative heat flux for various wettability-patterned surfaces. (c) Heat flux versus the heat transfer coefficient (HTC) for various patterned surfaces at point 4 of the RTD sensor (Reynolds number, Re: 6,000).

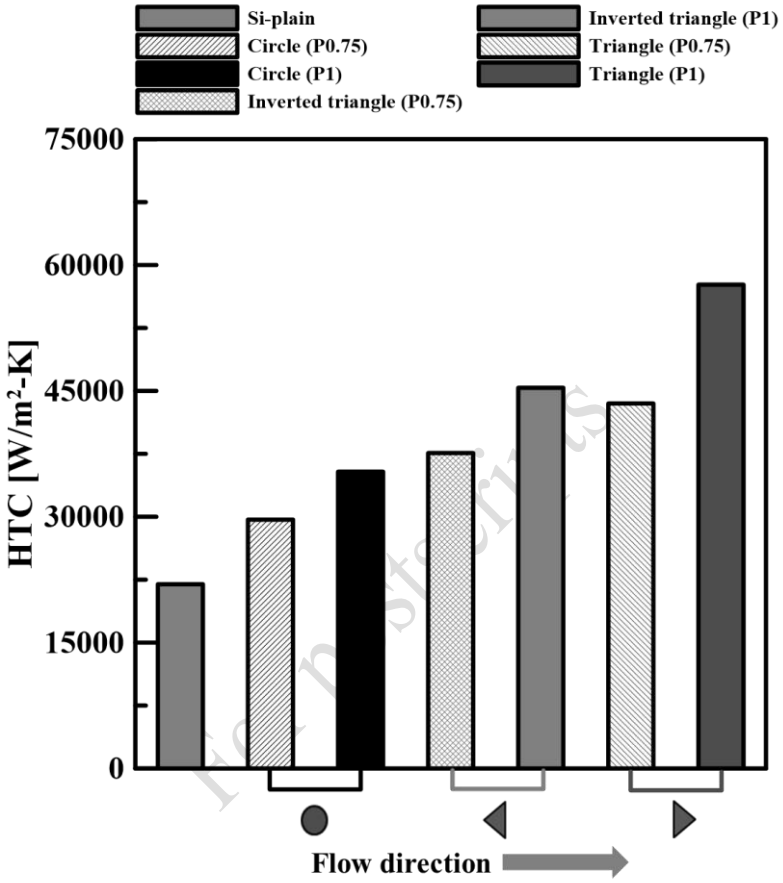

Figure 6 Comparison of the HTC between the wettability-patterned surfaces and the Si surface.

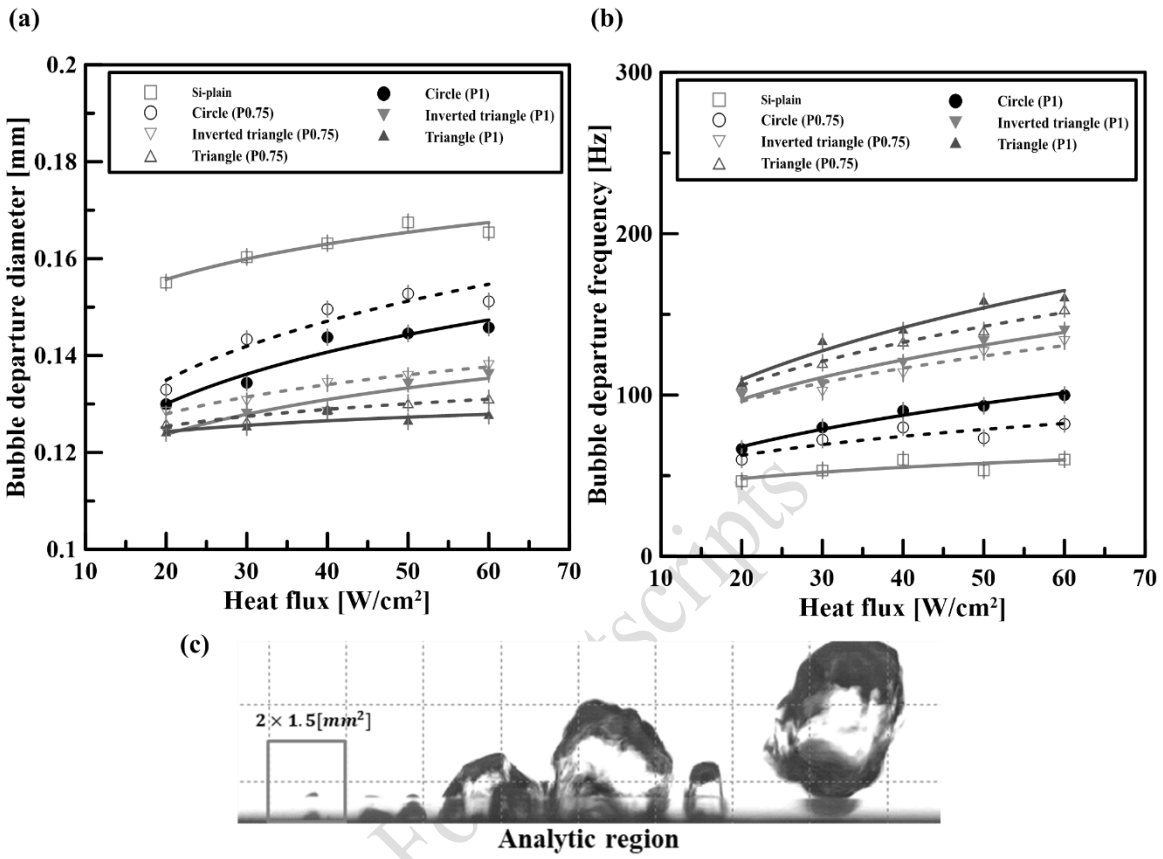

Figure 7 Bubble detachment characteristics for the wettability-patterned surfaces at Re = 6,000. Relationship between (a) the bubble departure diameter and the relative heat flux and (b) the bubble departure frequency and the relative heat flux. (c) Analytic region of upstream bubble characteristics along the flow direction.

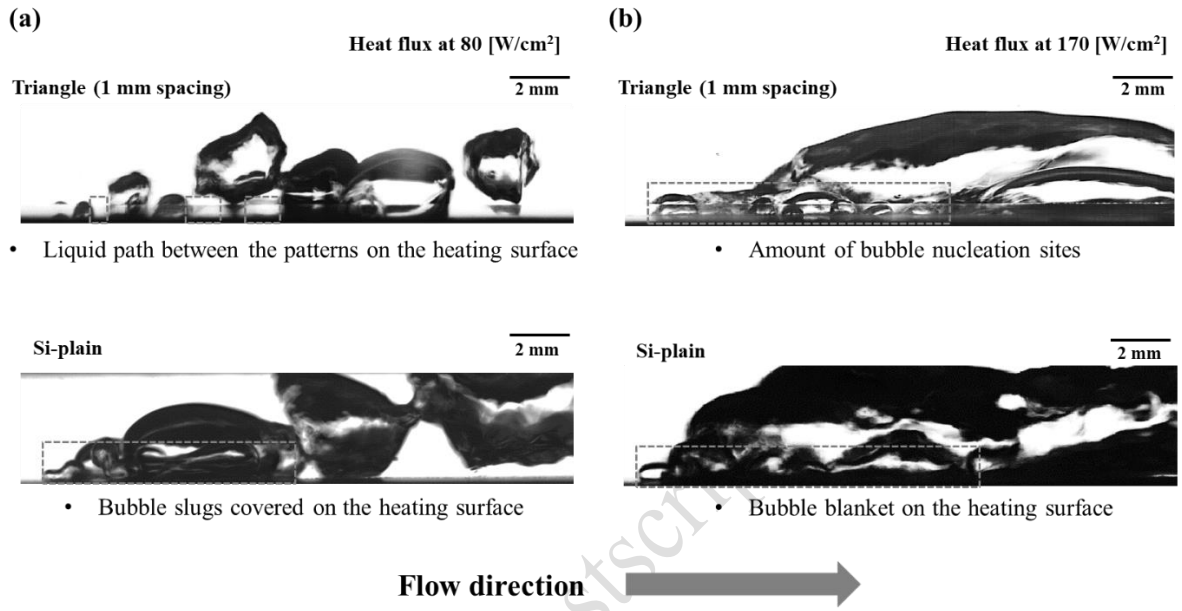

Figure 8 Bubble detachment from the wettability-patterned surfaces with 1-mm spacing with heat flux of (a) 80 and (b) 170 W/cm^2.

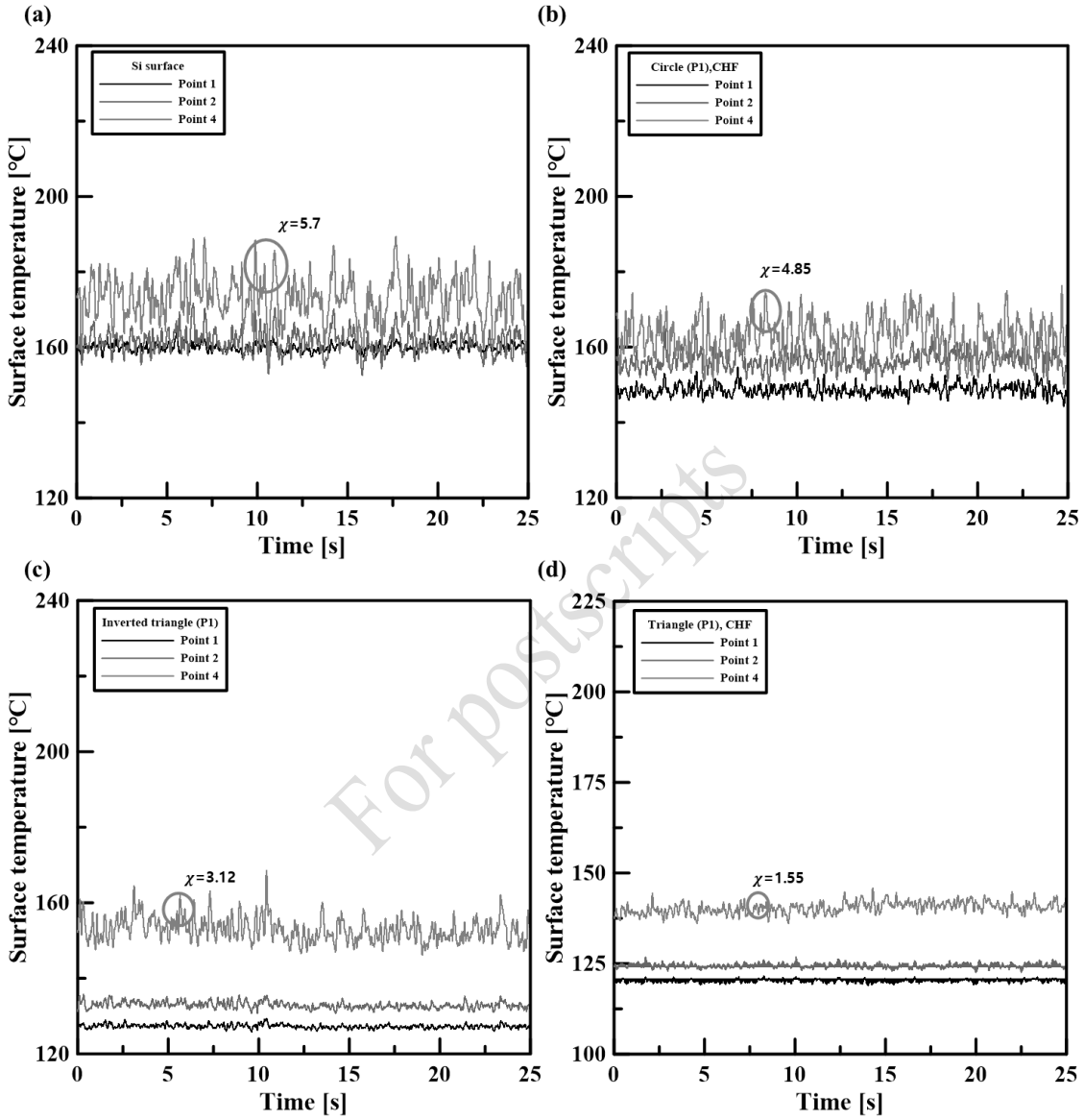

Figure 9 Temporal surface temperature for wettability-patterned surfaces with 1-mm spacing at various points of the RTD sensor: (a) Si surface and hydrophobic-patterned surfaces having a (b) circle, (c) inverted triangle, and (d) triangle pattern.

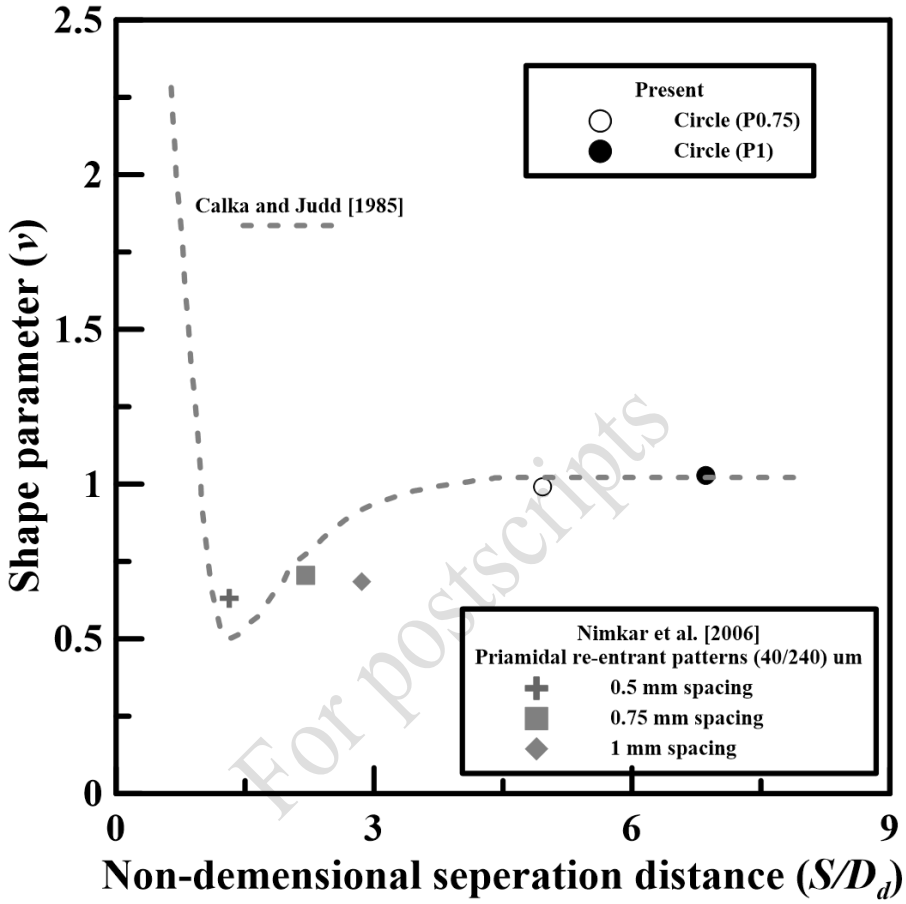

Figure 10 Relationship between the shape parameter and the non-dimensional separation distance for various wettability-patterned surfaces.

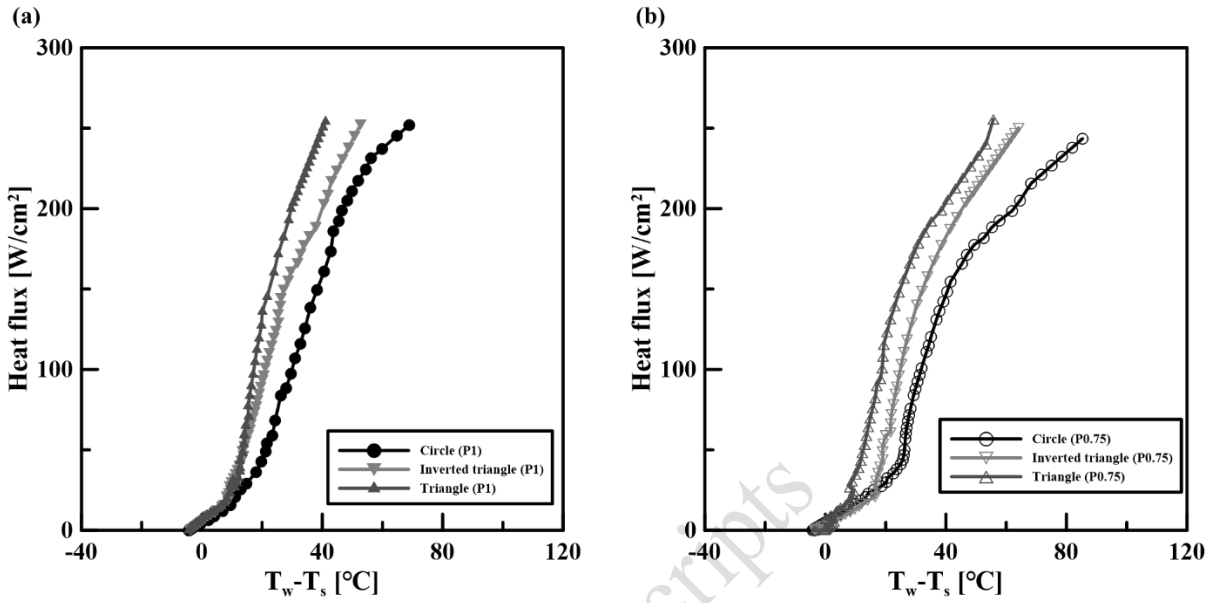

Figure 11 Relationship between wall superheat and the relative heat flux for various wettability-patterned surfaces at Re = 6,000. Patterned surfaces with a (a) 0.75-mm and (b) 1.0-mm inter-spacing.

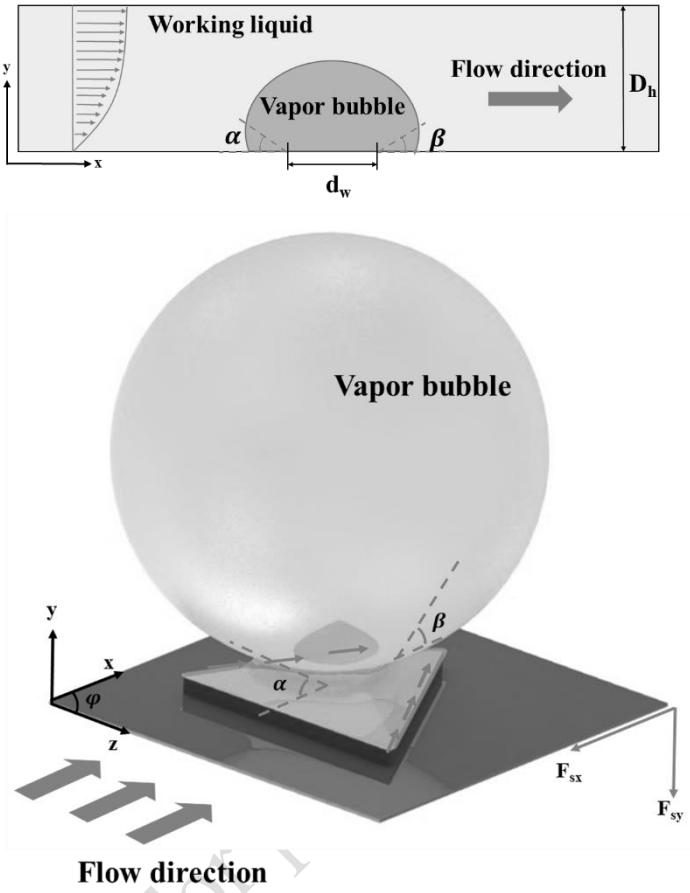

Figure 12 Schematic diagram of the bubble lift force acting on a single hydrophobic pattern in a horizontal conventional channel.

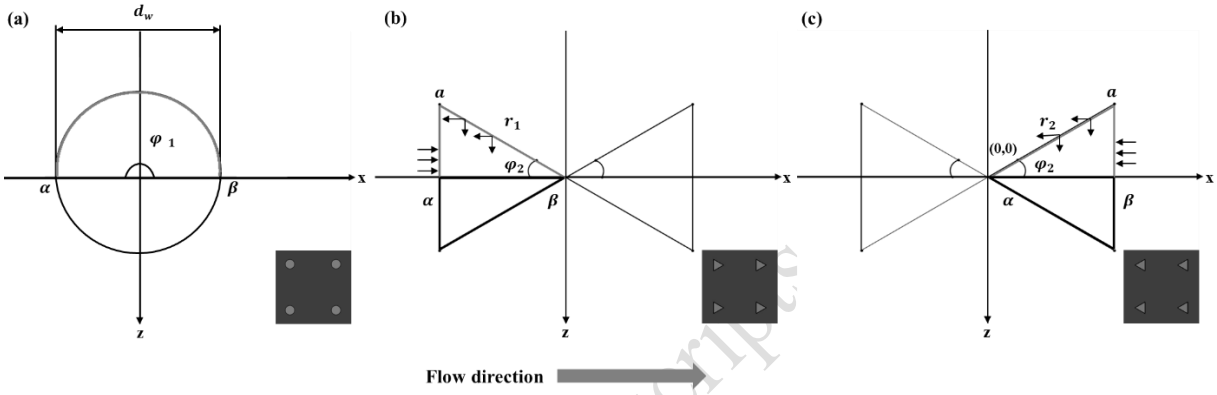

Figure 13 Schematic diagram of the shape effect of hydrophobic patterns on bubble lift force in the flow direction: (a) circle, (b) triangle, and (c) inverted triangle hydrophobic patterns.

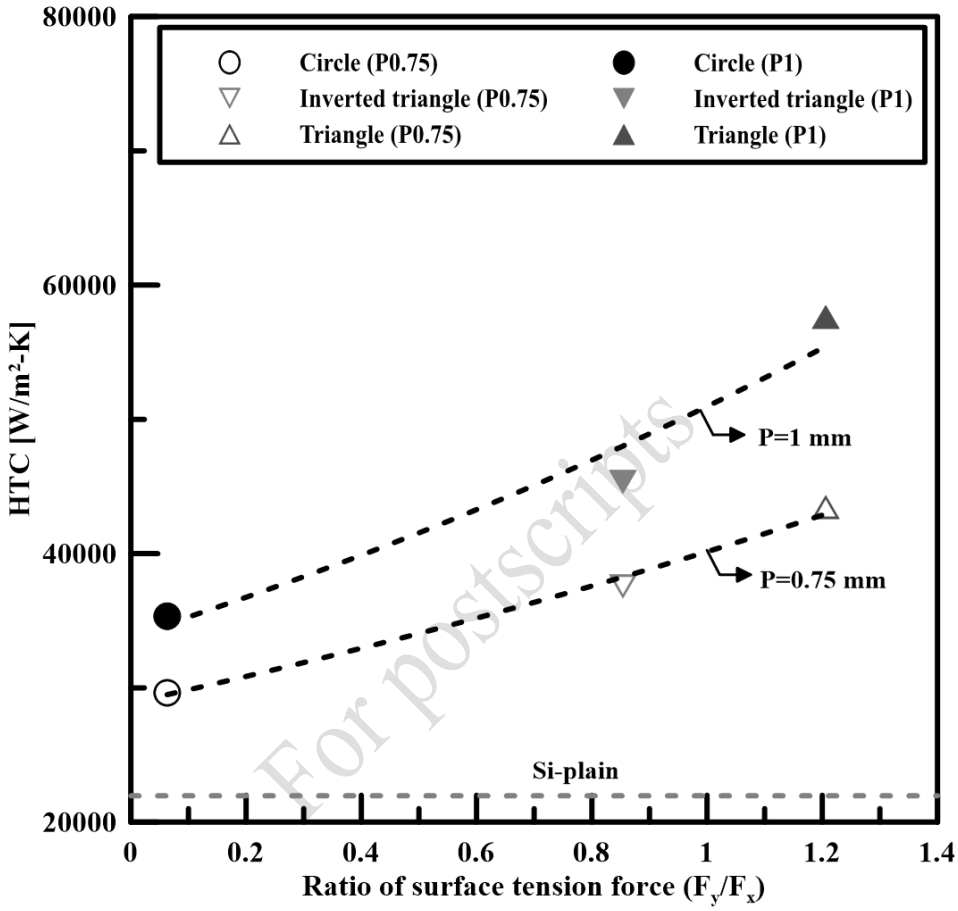

Figure 14 Relationship between the bubble lift force and the HTC for the wettability-patterned surfaces (Re = 6,000).

Answers to the 1st Reviewer's Comments

We appreciate the significant efforts that reviewers put into our paper to review. We will respond to the reviewer′s comments and suggestions in detail in the following. According to the reviewer′s opinion, we modified the manuscript with notification by highlighting and attached a full list of changes.

Reviewer #1

(1)
Why the investigated inter-spacing is 0.75 or 1 mm? Can the authors provide a universal principle to predicate or design the inter-spacing?

(Reply)

The authors thank the reviewer for raising the point. The design basis of the inter-spacing between two neighboring hydrophobic patterns was based on our previous work proposed by Lee et al. [34], they created micro-nano hybrid surfaces (MNHS) to enhance the overall boiling heat transfer performance and improve thermal stability by delaying bubble coalescence occurrence and catalyzing bubble nucleation under pool boiling conditions. The experimental results indicated that when the inter-spacing between the MNHS surfaces was at 1 mm, the critical heat flux (CHF) can be significantly improved by more than 170% as compared to a bare silicon surface, as shown in Fig. R1.

In addition, the influence of thermal interactions would become stronger when the inter-distance between two neighboring hydrophobic patterns decreased, resulting in a premature bubble coalescence before fully-development of bubbles, thereby preventing the recirculation of cooling liquid from reaching heated surfaces, as shown in Fig. R2. This is in agreement the findings of Sujith et al. [22], where the promotive effect of bubble nucleation on adjacent nucleation sites existed only if the inter-spacing between two neighboring hydrophobic patterns was sufficiently small, and therefore, to further determine the influence of inter-spacing between adjacent nucleation sites on bubble characteristics, we created surfaces consisted of a hydrophilic substrate and hydrophobic patterned arrays in various shapes with 0.75- and 1-mm inter-spacings as the test surfaces in this study, accordingly.

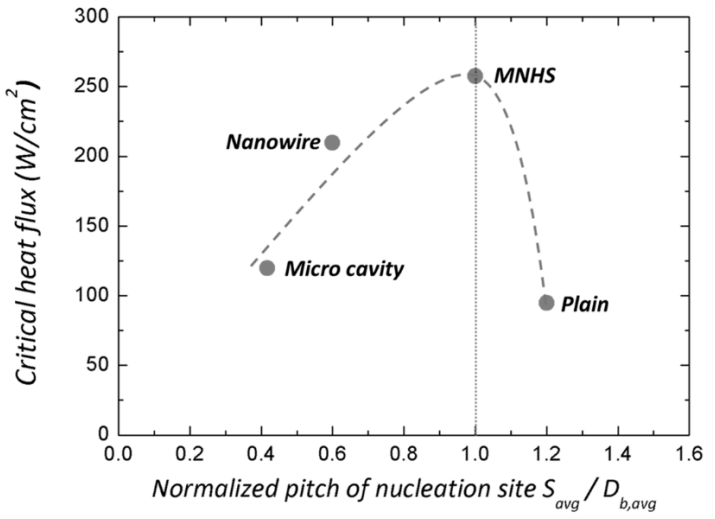

Figure R1 CHF as a function of normalized pitch of nucleation sites for various test surfaces, i.e., the red dashed line represented that the dimension of inter-spacing between nucleation sites is same with the averaged bubble departure diameter [34].

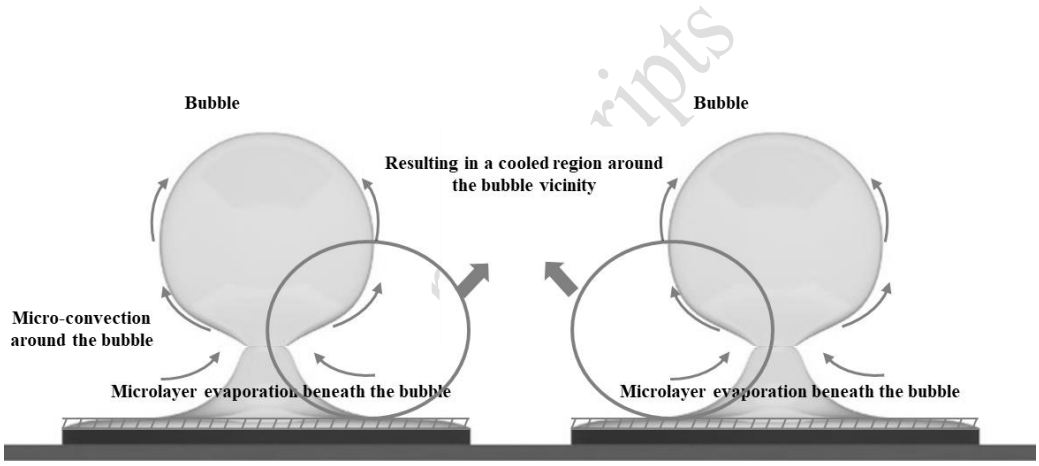

Figure R2 Schematic diagram of the influence of inter-spacing between two neighboring hydrophobic patterns on bubble nucleation.

- **Added reference in revised manuscript**

[34] Lee, D., Lee, N., Shim, D. I., Kim, B. S. & Cho, H. H. Enhancing thermal stability and uniformity in boiling heat transfer using micro-nano hybrid surfaces (MNHS). Applied Thermal Engineering 130 (2018), 710–721.

(2)

What is the accuracy of experimental equipment in the visualization of bubbles? What is the resolution? This needs to be clarified. The calculation of the overall uncertainty needs further explanation.

(Reply)

As the referee pointed out the lack of illustration on the uncertainty of measured bubbles, which is very important, especially in analyzing bubble characteristics on heated surfaces in the present study. The bubble detachment characteristics on heated surfaces were conducted on surfaces consisted of the hydrophilic substrate and the hydrophobic patterned arrays with various shapes using a high speed camera (Speedsense M310, Dantec, Denmar) with an 100W LED light source based on the shadowgraph method. All the required measurements regarding images of fully-detachment bubbles was analyzed by a commercial software (version 3.30, Dynamic Studio, Denmark) to determine the equivalent bubble departure diameter. The software analyzes the equivalent diameter of fully-departing bubbles by assuming that the recorded 2D image of the bubble is a perfect circle. The equation for the equivalent diameter of departing bubbles is given by

$$d_b = 1.55 \cdot \frac{A_b^{0.625}}{p_b^{0.25}}$$

where A_b and P_b are the cross-sectional area and perimeter of the fully-detachment bubble, respectively [32].

For further determining the pixel uncertainty in the bubble diameter based on the shadowgraph method, we conducted a visualization test on 3 glass marbles using the high-speed camera and the 100W LED light source to represent departing bubbles that recorded with a shutter speed of 8000 frame/s. The test chamber was fully-filled with the degassed deionized water and the working temperature was at saturated conditions, as shown in Fig. R3. The relative measured results of equivalent diameter of glass marbles are concluded in Table 1, which indicated that the standard deviation of the measured diameter of glass marble varied over a range of 00067-0.0068 mm and the best accuracy of the detected diameter of glass marbles was within a range of 0.1 mm, thus the pixel uncertainty in the bubble diameter that obtained from the bubble visualization was determined as $\pm$0.1 mm in this study.

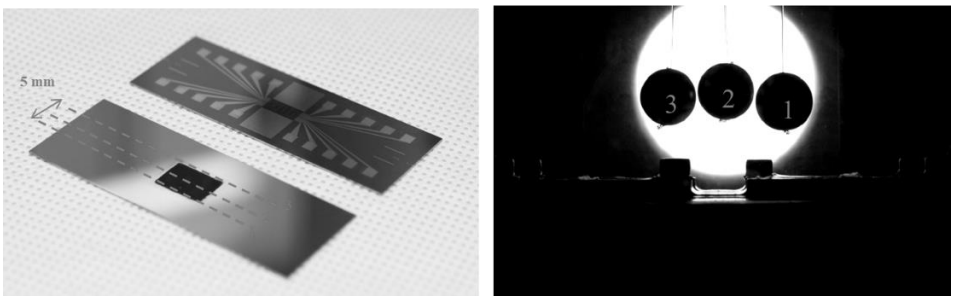

Figure R3 Uncertainty of equivalent diameter of glass marbles using shadowgraph method.

Table 1 Measured results of glass marbles based on a shadow graph method.

Number	Averaged diameter [mm]	Standard deviation [mm]	Maximum uncertainty [mm]
1	14.08	0.0067	+0.1
2	13.97	0.0067	-0.1
3	13.86	0.0068	-0.1

- **Added sentences in revised manuscript (page 9, line 3)**

"In addition, the bubble detachment characteristics on heated surfaces were conducted on surfaces consisted of the hydrophilic substrate and the hydrophobic patterned arrays with various shapes using a high speed camera (Speedsense M310, Dantec, Denmar) with an 100W LED light source based on the shadowgraph method in this study. All the required measurements regarding images of fully-detachment bubbles was analyzed by a commercial software (version 3.30, Dynamic Studio, Denmark) to determine the equivalent bubble departure diameter. By assuming that the measured 2D image of the bubble is a perfect circle, the software is able to analyze the equivalent diameter of fully-departing bubbles. The equation for the equivalent diameter of departing bubbles is given by

$$d_b = 1.55 \cdot \frac{A_b^{0.625}}{p_b^{0.25}}$$

where A_b and P_b are the cross-sectional area and perimeter of the fully-detachment bubble, respectively [31]."

- **Added sentences in revised manuscript (page 11, last paragraph)**

"The pixel uncertainty in the bubble diameter that obtained from the bubble visualization was ±0.1 mm [36, 37]."

- **Added reference in revised manuscript**

[31] Koch P, Equivalent diameters of rectangular and oval ducts, Build Serv. Eng. Res. Technol. 29 (2008),341-347.

[36] Peyghambarzadeh, S. M., Hatami, A., Ebrahimi, A. & Fazel, A. Photographic study of bubble departure diameter in saturated pool boiling to electrolyte solutions. Chemical Industry and Chemical Engineering Quarterly 20, 143–153 (2014).

[37] Lee, D., Lee, N., Shim, D. I., Kim, B. S. & Cho, H. H. Enhancing thermal stability and uniformity in boiling heat transfer using micro-nano hybrid surfaces (MNHS). Applied Thermal Engineering 130 (2018), 710–721.

(3)

At bubble departure behavior too there is extensive literature on this topic. The analysis should be further in-depth. For example: doi:10.1016/j.ijheatmasstransfer.2017.11.145. and doi:10.1115/1.4040147 must be cited.

(Reply)

The reviewer raised a notable concern. Depending on the working conditions, bubble characteristics can be the dominant flow boiling heat transfer mechanisms, thus an appropriate analysis of bubble departure behavior can help the authors and readers to determine the cooling mechanisms of flow boiling by analyzing bubbles that form on heated surfaces. According to a previous work proposed by Kandlikar et al. [28], they suggested a criterion for classifying the categories of flow channels from convectional channels to molecular nanochannels, depending on the hydraulic diameter of test chambers. For the bubble departure behavior in microchannels [29, 30], the bubble development process from the confined bubble slug to the annular flow can be observed as well as the region of partial dry-out on heated surfaces from the top of flow channels as the heat flux gradually elevated. On the other hand, the hydraulic diameter of the rectangular test section was 5 mm and the length of the main channel was 375 mm in the present work, indicating that the test section was the convectional channel, which was relatively larger than those of the microchannel, resulting in different bubble characteristics on heated surfaces. Particularly, the bubble characteristics can be only observed at the sides of the test section and the heated area was designed in 5 mm in width and 10 mm in length in this study, which was relatively small when compared with the test section, thus we only focused on the bubble detachment behavior on heated surfaces including the bubble departure diameter and the liquid path instead of the confined flow pattern of bubble owing to the limitations of experimental equipment in this study.

- **Added sentences in revised manuscript (page 9, line 7)**

"Depending on the working conditions, the flow boiling heat transfer mechanism is strongly dependent on bubble characteristics, thus an appropriate analysis of bubble departure behavior can help the authors and readers to determine the cooling mechanisms of flow boiling by analyzing bubbles that form on heated surfaces. According to a previous work proposed by Kandlikar et al. [28], they suggested a criterion for classifying the categories of flow channels from convectional channels to molecular nanochannels depending on the hydraulic diameter of test chambers. For the bubble departure behavior in microchannels [29, 30], the bubble development process from bubble slug to the confined annular flow can be observed as well as the region of partial dry-out on heated surfaces from the top of flow channels as the heat flux gradually elevated. On the other hand, the hydraulic diameter of the rectangular test section was 5 mm and the length of the main channel was 375 mm in the present work indicating that the test section was the convectional channel, which was relatively larger than those of the microchannel, resulting in different bubble characteristics on heated surfaces. Moreover, the bubble characteristics can be only observed at the sides of the test section and the heating area was designed in 5 mm in width and 10 mm in length, which was relatively small when compared with the test section, thus we only focused on bubble departure characteristics on heated surfaces such as bubble departure diameter and liquid paths instead of the confined flow patterns of bubbles due to the

limitations of the experimental equipment.″

- **Added reference in revised manuscript**

[28] Kandlikar, S. G. & Grande, W. J. Evolution of Microchannel Flow Passages–Thermohydraulic Performance and Fabrication Technology. Heat Transfer Engineering 24 (2003), 3–17.

[29] Li, W., Zhou, K., Li, J., Feng, Z. & Zhu, H. Effects of heat flux, mass flux and two-phase inlet quality on flow boiling in a vertical superhydrophilic microchannel. International Journal of Heat and Mass Transfer 119 (2018), 601–613.

[30] Li, W., Luo, Y., Zhang, J. & Minkowycz, W. J. Simulation of Single Bubble Evaporation in a Microchannel in Zero Gravity with Thermocapillary Effect. J. Heat Transfer 140 (2018).

(4)

"the experimental results for the wettability-patterned surfaces were not within the valid range" is mentioned. Is the selected experimental data meaningful under pool boiling conditions?

(Reply)

The authors thank the reviewer for raising the point. Fig 10 shows the relationship between the shape parameter and the non-dimensional separation distance for various wettability-patterned surfaces. We selected surfaces consisted of circular hydrophobic-patterned arrays and a hydrophilic substrate, with 0.75-and 1-mm inter-spacing as the representative cases. The present results, which were conducted under flow boiling conditions using saturated deionized water at atmospheric pressure, were compared to the experimental data of Nimkar et al. [17], which were obtained under pool boiling conditions, using the empirical correlation proposed by Calka et al. [38]. In Fig. 10, the present experiment empirically assessed the correlation region for $S/D_d > 3$ because bubble formation was suppressed by the convective working fluid resulting in a relatively small mean diameter of departing bubbles and a shift to the right of the value of the non-dimensional separation distance.

The text regarding the effect of inter-spacing on bubble nucleation has been rewritten for avoiding confusion.

- **Revised sentences in revised manuscript (page 15, line 9)**

~~"Hence, the experimental results for the wettability-patterned surfaces were not within the valid range."~~

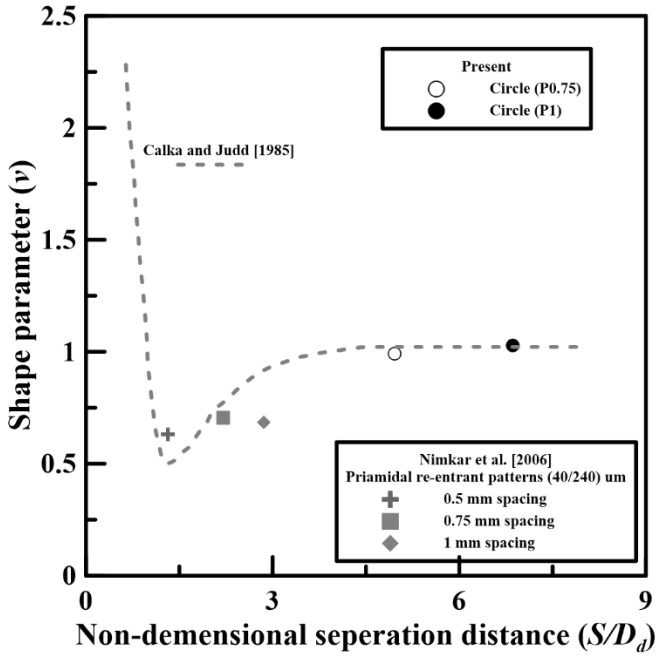

Figure 10 Relationship between the shape parameter and the non-dimensional separation distance for various wettability-patterned surfaces.

(5)

Figure 8b: Bubble behavior on the test surfaces was difficult to characterize directly

(Reply)

An important observation was made by the reviewer. When the heat flux increased within a specific high heat flux region (before dry-out occurrence), bubble characteristics on the wettability-patterned surfaces were more difficult to resolve, owing to irregular bubbles that vigorously merged and moved along the heated surface. Nevertheless, bubble nucleation sites on the wettability-patterned surfaces were still observed via bubble visualization, even in the high heat flux region [20]. Based on these results, we also determined that several bubble nucleation sites formed on the wettability-patterned surfaces consisted of triangle-shaped hydrophobic-patterned arrays, whereas the entire heated surface of the Si-surface was continuously covered by vapor blankets when the heat flux was raised to 170 W/cm^2, in an attempt to identify the difference of bubble characteristics between the wettability-patterned surface and the bare Si-surface.

In Fig. 8(b), the surface consisted of triangle hydrophobic patterned arrays have revised using bubble images that extracted from the same visualization result, and the video clips regarding the bubble characteristics on the bare Si-surface and the wettability patterned surface were also attached in the revised Supplementary material, respectively.

- **Revised figure in revised manuscript**

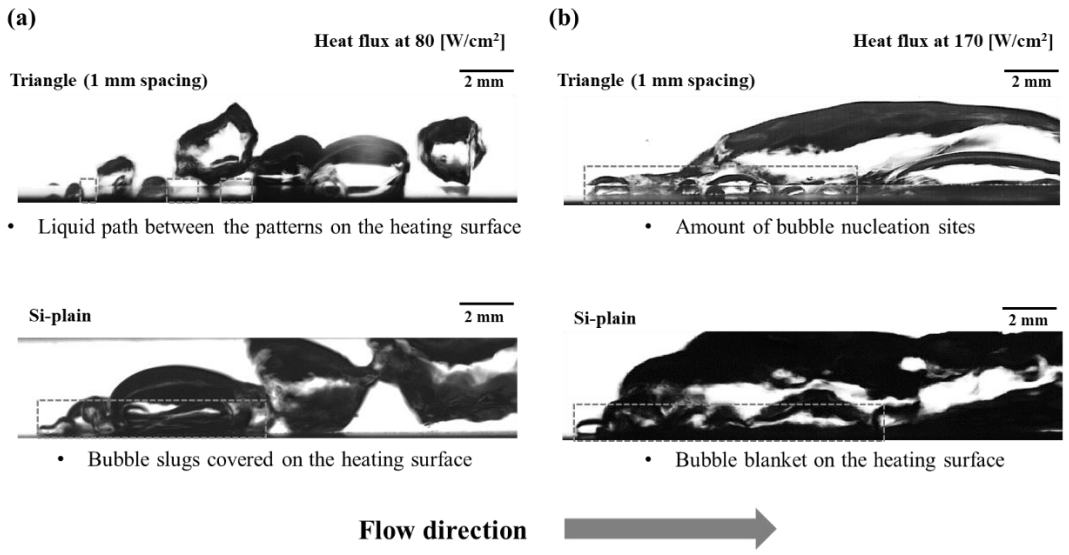

Figure 8. Bubble detachment from the wettability-patterned surfaces with 1-mm spacing with heat flux

of (a) 80 and (b) 170 W/cm^2.

Added videos in Supplementary material

Supplementary video 1_Triangular patterned surface

Supplementary video 2_Bare Si-surface

(6)

"In this study, we assumed that the bubble dynamic contact angles and were 50 ° and 40°" is mentioned. What is the basis of the assumption?

(Reply)

The assumption of the bubble dynamic contact angles was based on the bubble visualization results in this study, we analyzed single departing bubble from the surfaces consisted of the hydrophilic substrate and the hydrophobic patterned arrays in triangular, inverted-triangular, and circular shapes with the 1-mm inter-spacing, respectively as the heat flux raised to 40 W/cm^2, as shown in Fig. S2 (a). Because of the bubble dynamic contact angles, which can be differentiated as advancing and receding contact angles (α and β), are difficult to determine especially within the downstream region of the heated surface along the flow direction, and thus we only analyzed bubbles that form on the upstream surface (i.e. the red analytic region), which was not merged or affected by the neighboring bubbles. According to Fig. S2 (b), the measured results in terms of the averaged advancing and receding contact angles on the wettability-patterned surfaces were over a range of 50-120 and 40-80 degrees, respectively. In addition, it is widely known that the advancing contact angle is generally larger than the receding contact angle along the flow direction under flow boiling conditions. As such, three groups of advancing and receding contact angles (i.e. α/β=50/40, 60/50, and 70/60) were selected as representative cases for determining the relationship between the heat transfer coefficient (HTC) and the relative bubble lift force on surfaces composed of hydrophobic patterned arrays with various shapes.

Fig. S2 (c) shows HTC as a function of the predicted ratio of bubble lift force on wettability-patterned surfaces with various group of the advancing and receding contact angles, the predicted results indicated that the surfaces with the triangular shape revealed the highest ratio of bubble lift force than those with the inverted-triangular and circular shapes, which corresponded to the experimental results, indicating that bubbles can be released more frequently on surfaces with triangle hydrophobic patterns and subsequently improved the HTC. For preventing the overprediction on the bubble lift forces on the wettability-patterned surfaces, we selected the minimum predicted ratio of bubble lift force as the representative case by assuming that the advancing and receding around a single bubble on the wettability-patterned surfaces were 50 and 40 degrees, respectively in this study.

- **Added sentences in revised manuscript (page 16, line 1)**

"The basis of the assumption of bubble dynamic contact angles is given in the supplementary

materials."

- **Added sentences in Supplementary material (page 2, line 1)**

"The assumption of the bubble dynamic contact angles was based on the bubble visualization results in this study, we analyzed single departing bubble from the surfaces consisted of the hydrophilic substrate and the hydrophobic patterned arrays in triangular, inverted-triangular, and circular shapes with the 1-mm inter-spacing, respectively as the heat flux raised to 40 W/cm^2, as shown in Fig. S2 (a). Because of the bubble dynamic contact angles, which can be differentiated as advancing and receding contact angles (α and β), are difficult to determine especially within the downstream region of the heated surface along the flow direction, and thus we only analyzed bubbles that form on the upstream surface (i.e. the red analytic region), which was not merged or affected by the neighboring bubbles. According to Fig. S2 (b), the measured results in terms of the averaged advancing and receding contact angles on the wettability-patterned surfaces were over a range of 50-120 and 40-80 degrees, respectively. In addition, it is widely known that the advancing contact angle is generally larger than the receding contact angle along the flow direction under flow boiling conditions. As such, three groups of advancing and receding contact angles (i.e. α/β =50/40, 60/50, and 70/60) were selected as representative cases for determining the relationship between the heat transfer coefficient (HTC) and the relative bubble lift force on surfaces composed of hydrophobic patterned arrays with various shapes.

Fig. S2 (c) shows HTC as a function of the predicted ratio of bubble lift force on wettability-patterned surfaces with various group of the advancing and receding contact angles, the predicted results indicated that the surfaces with the triangular shape revealed the highest ratio of bubble lift force than those with the inverted-triangular and circular shapes, which corresponded to the experimental results, indicating that bubbles can be released more frequently on surfaces with triangle hydrophobic patterns and subsequently improved the HTC. For preventing the overprediction on the bubble lift forces on the wettability-patterned surfaces, we selected the minimum predicted ratio of bubble lift force as the representative case by assuming that the advancing and receding around a single bubble on the wettability-patterned surfaces were 50 and 40 degrees, respectively in this study.

"

Added figure in Supplementary material

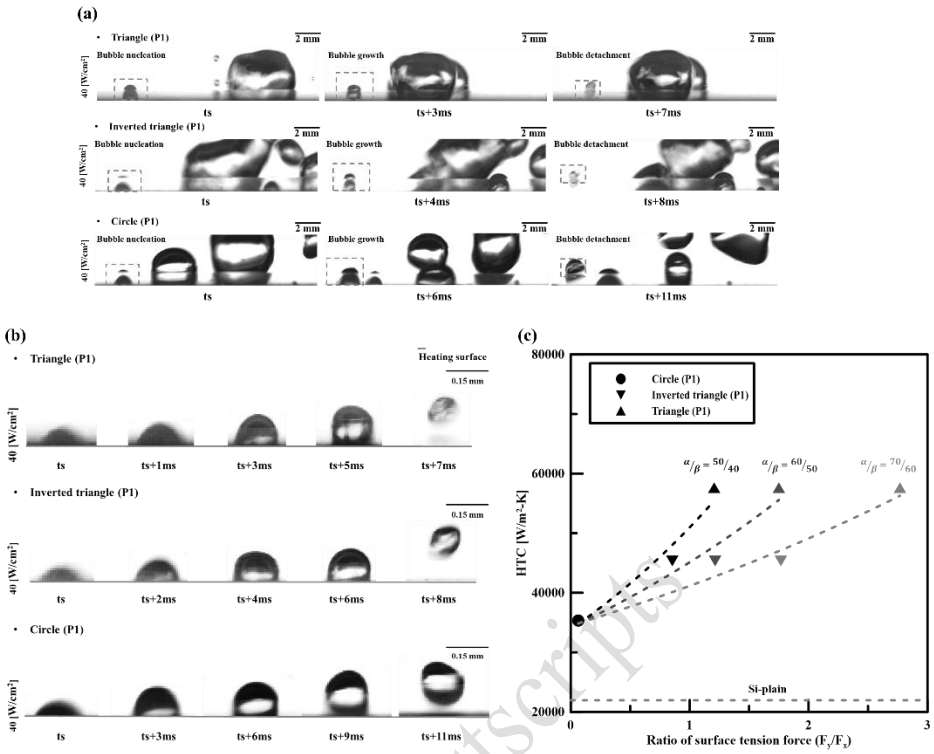

Figure S2 (a) Tracking regions of single departing bubble (b) Bubble detachment process and (c) HTC versus ratio of surface tension force on surfaces consisted of hydrophobic patterned arrays in triangular, inverted-triangular, and circular shapes with inter-spacing of 1 mm.

Answers to the 2nd Reviewer's Comments

We appreciate the significant efforts that reviewers put into our paper to review. We will respond to the reviewer′s comments and suggestions in detail in the following. According to the reviewer′s opinion, we modified the manuscript with notification by highlighting and attached a full list of changes.

(Reviewer #2)

(1) Double-check the contact angle values when presenting the surface tested by Kim et al. [24] (Introduction, fifth paragraph).

(Reply)

We apologize for supplying the incorrect information of contact angle values in the previous work proposed by Kim et al. [24], the detail information of the contact angles for hydrophobic and hydrophilic surfaces have thoroughly checked and the sentences in the revised manuscript also corrected accordingly.

- **Revised sentences on page 3, line 21**

"Kim et al. [24] experimentally explored the influence of heterogeneous wetting surfaces on flow boiling performance in a vertical macro-channel (D_h = 7.5 mm), in which wettability-patterned surfaces were combined with hydrophobic patterns (coated with Teflon; θ_c = 120°) and a hydrophilic surface (coated with SiO_2; θ_c = 57°)."

- **Reference for revision**

[24] Kim, J. M. et al. Effect of heterogeneous wetting surface characteristics on flow boiling performance. International Journal of Heat and Fluid Flow 70 (2018), 141–151.

(2)

Clearly state the dimensions (height and width) of the rectangular channel (dh = 5mm). From Fig. 2, the reader has to assume that the heating width is the same as the channel width to determine the channel height.

(Reply)

As the reviewer commented, the dimensions of the rectangular channel should be more specifically stated in this study. The height and the width of the rectangular channel are 5 mm, respectively.

The sentences have been rewritten and Fig. 2 was also modified in the revised manuscript.

- **Revised sentences in revised manuscript (page 7, line 25)**

"(i.e., the height and the width of the channel are 5 mm, and D_h= 5 mm)"

- **Revised figure in revised manuscript (page 32, line 1)**

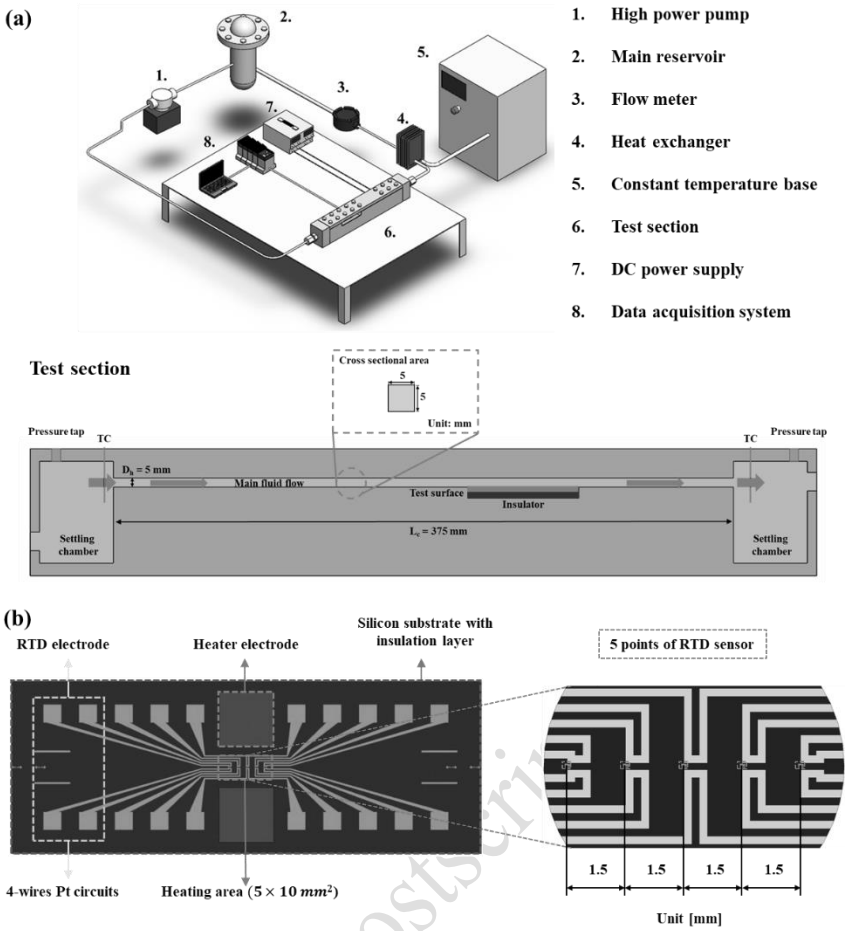

Figure 2 Experimental setup. (a) Flow boiling experimental apparatus. (b) Resistance temperature detector (RTD) sensor.

(3)

How was the saturation temperature determined? As the authors state that the experiments were conducted at atmospheric pressure, however, the flow loop would generate pressure head (e.g., magnetic pump and test section) and thus elevate the absolute pressure and saturation temperature at the test section. Was any pressure head generated by the flow loop considered negligible? Also, as the generation of bubbles increases (or increase in heat flux), the pressure drop in the test section will increase, leading to higher pressure in the flow loop. Was this pressure increase accounted for saturation temperature?

(Reply)

As the reviewer pointed out, the pressure head would generate by the magnetic pump and the test section, escalating both the absolute pressure and the saturation temperature of the test section. In order to maintain the working fluid at atmospheric pressure, we used a pressure valve, which was installed at the top of the water storage tank, to regulate the atmospheric pressure condition (i.e., the pressure valve was opened after a 2 hours-degassing procedure). Furthermore, the water storage tank was fully-filling up by degassed DI water to avoid air space occurrence that could affect the operational conditions of the working fluid during the experiment. Therefore, the pressure head generated by the experimental equipment would be considered negligible, accordingly.

In terms of the saturated condition of the working fluid, the temperature of the working fluid raised with additional bubbles that form on heated surfaces, which increased the pressure drop in the flow loop as the liquid passed through the test channel, while the authors focused on local flow boiling heat transfer characteristics in this study. The fluid temperature was maintained less than the saturation condition of water to ensure the working fluid in a completely liquid phase because of some vaporization was occurred in the working fluid after passing the heat exchanger (Model 131001694) when the fluid temperature increased nearly at 100°C. In addition, the inlet temperature of the working fluid was regulated by the heat exchanger and maintained at 98.5±0.6°C, which allowed for saturated flow boiling [Ref. 1], as shown in Fig. R1. The amount of temperature deviation of 0.6 °C is reasonable as compared to the other findings of Megahed et al. [Ref. 2]. Therefore, the authors used the averaged fluid temperature at the inlet and outlet of the channel as a bulk fluid temperature to evaluate the local boiling heat transfer characteristics and all the experiments regarding the wettability-patterned surfaces were investigated in the saturated condition in this study.

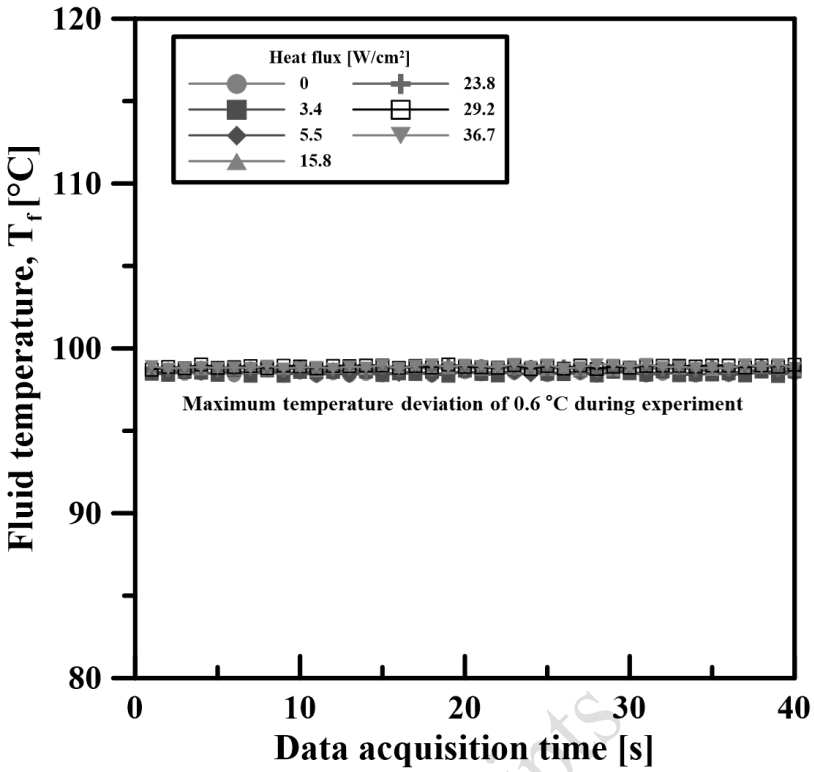

Figure R1 Averaged fluid temperature distribution on surfaces consisted of triangular hydrophobic patterned arrays at inlet and outlet of the test channel as elevating heat flux.

- **Revised sentences in revised manuscript (page 7, line 19)**

"the main reservoir (i.e., a pressure valve was installed at the top of the main reservoir to regulate the pressure conditions)."

- **Reference for revision**

[Ref. 1] Lee, P.-S. & Garimella, S. V. Saturated flow boiling heat transfer and pressure drop in silicon microchannel arrays. International Journal of Heat and Mass Transfer 51 (2008), 789–806.

[Ref. 2] Megahed, A. Local flow boiling heat transfer characteristics in silicon microchannel heat sinks using liquid crystal thermography. International Journal of Multiphase Flow 39 (2012), 55–65.

(4)

The authors indicated that the fluid temperature entering the test section is regulated by a heat exchanger but failed to state the fluid inlet temperature at the test section clearly. From Fig. 5(b), it is apparent that the subcooling varies from 2°C to 10°C for all tested surfaces even though at the same flow conditions (0.51kg/min). This variation of subcooling at the same flow rate would lead to different incipience behavior and nucleation density value and also affect the bubble detachment pattern.

(Reply)

The authors thank the reviewer for raising a notable concern, we used the averaged fluid temperature at the inlet and outlet of the flow channel as the bulk fluid temperature to evaluate the local flow boiling heat transfer characteristics in this study. The heat exchanger (Model 131001694) was used to maintain the working fluid near the saturated temperature of DI water, which is 100℃. In addition, all the experiments regarding wettability-patterned surfaces were conducted with the working temperature at 98.5±0.6℃. We apologize for inaccurately plotting the experimental results in terms of the incipience point, the experimental data have thoroughly checked and modified with Fig. 5(b) and (c), accordingly.

- **Revised sentences in revised manuscript (page 7, line 20)**

"A heat exchanger (Model 131001694) was used to regulate the fluid inlet temperature at 98.5±0.6℃, which was closed to the saturation temperature of DI water before pumping the saturated fluid into the test section. In addition, the averaged fluid temperature at the inlet and outlet of the test section was treated as a bulk fluid temperature on the heated surface under saturated condition."

- **Revised figure in revised manuscript (page 36, line 1)**

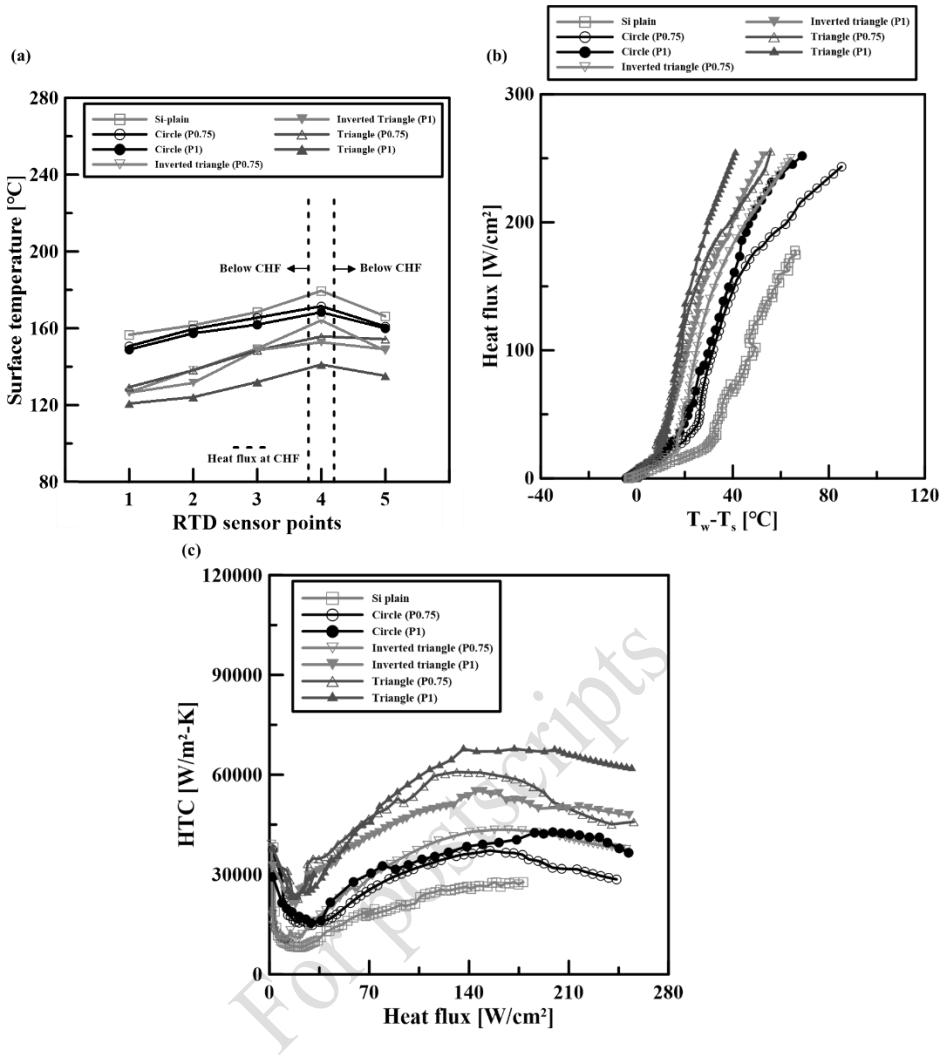

Figure 5 Boiling characteristics on test surfaces in terms of (a) heat flux versus wall superheat and (b) heat transfer coefficient as a function of heat flux.

(5)

Is the temperature distribution in Fig. 5(a) at a specific heat flux (e.g., nearly CHF)? If not at a particular heat flux, is the phenomenon shown in this figure applicable to all heat fluxes?

(Reply)

The authors thank the reviewer for raising the point. The heat flux for various test surfaces in terms of the temperature distribution was nearly the CHF, as shown in Fig. 5 (a). A similar trend of temperature distribution can be also observed on the surface consisted of the hydrophilic substrate and the hydrophobic patterned arrays in the triangular shape with 1-mm inter-spacing within various heat flux regions, as shown in Fig. R2. By varying the heat flux from onset of nucleation boiling (ONB) to a middle heat flux (100 W/cm^2), the surface temperature gradually increased in the upstream region from point 1 to point 4 and then decreased in the downstream region from point 4 to point 5, which can be attributed to merged bubbles detachment behavior on the heated surface. Herein, the temperature gradient on the heated surface was within a range of ΔT_1= 1-4°C and the surface temperature at point 4 was the highest as compared with the other measured points of RTD sensors; while the similar phenomenon of temperature distribution on the test surfaces became more remarkable over the heat flux range of 104-255 W/cm^2, resulting in a large temperature gradient of ΔT_2= 2-21°C on the heated surface. Hence, the surface temperature distribution on test surfaces can be applicable to the heat flux region over ONB to CHF in this study.

The sentences regarding context of the surface temperature distribution have been rewritten in the revised manuscript.

- **Revised sentences in revised manuscript (page 13, line 12)**

"In addition, the surface temperature distribution on test surfaces can be applicable to specific heat flux regions over ONB to CHF in this study."

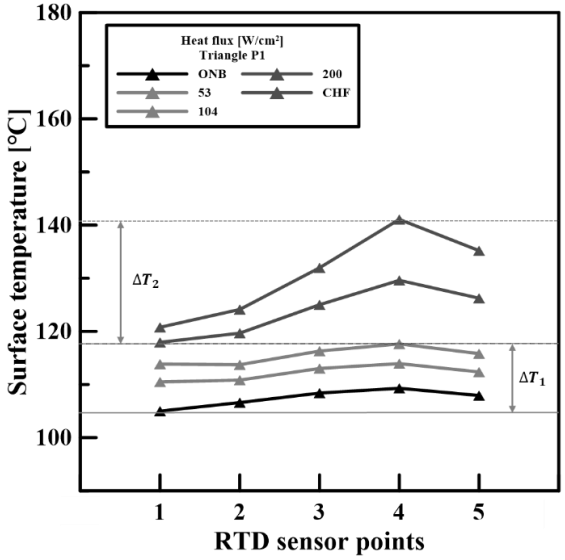

Figure R2 Surface temperature distribution over the local sensor points of the RTD sensor for surface consisted a hydrophilic substrate with triangle hydrophobic patterned with 1-mm inter-spacing.

(6)

The authors stated that the CHF crisis might occur at point 4 as the tested surface have a local maximum, as shown in Fig. 5(a). When examining the temporal temperature readings, was the CHF criteria (a 20°C temperature spike) first observed at point 4?

(Reply)

The reviewer raised a notable concern, even though a local maximum temperature appeared at point 4, the boiling crisis could occur at other measured points of RTDs among the test surfaces, thus a further examining in terms of the CHF criteria at all measured points was conducted on a surface consisted of the hydrophilic substrate and hydrophobic patterned arrays in the circular shape with 1-mm inter-spacing, as shown in Fig. R3. Among all measured points of RTDs, a remarkable temperature fluctuation can be observed over the region of point 3 to point 5, indicating that bubble coalescence occurred vigorously and the boiling crisis might take place in the downstream region on the heated surface. Particularly, a 20℃ temperature spike was first observed markedly at point 4 as the heat flux reached the CHF crisis, thus the experimental results regarding flow boiling heat transfer on wettability-patterned surfaces were redacted based on the experimental data at point 4, accordingly.

- **Revised sentences in revised manuscript (page 13, line 11)**

"(i.e., a 20℃ temperature spike was first observed markedly at point 4)."

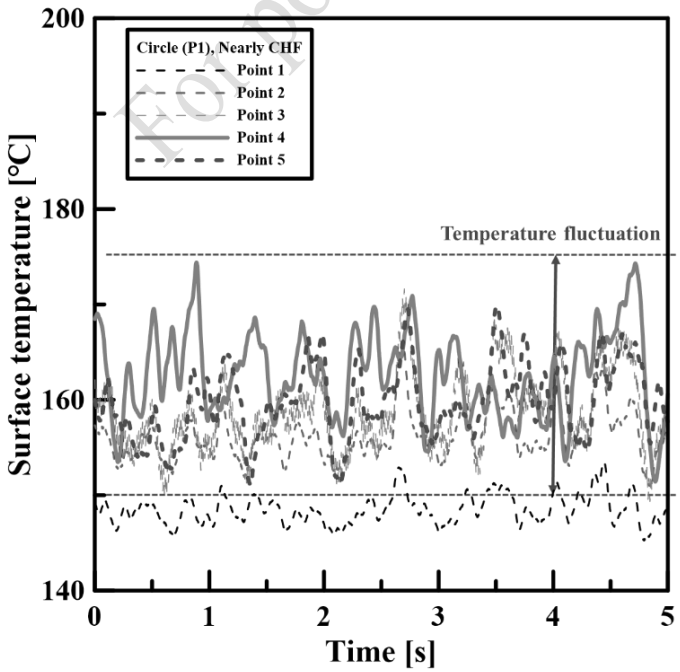

Figure R3 Temporal surface temperature on surfaces composed of circular hydrophobic patterns with 1-mm inter-spacing at all points of RTD sensor.

(7)

The authors assumed that the bubble dynamic contact angles and were 50° and 40°, respectively, for the analysis. Were those values randomly selected, or was there a specific reason?

(Reply)

The assumption of the bubble dynamic contact angles was based on the bubble visualization results in this study, we analyzed single departing bubble from the surfaces consisted of the hydrophilic substrate and the hydrophobic patterned arrays in triangular, inverted-triangular, and circular shapes with the 1-mm inter-spacing, respectively as the heat flux raised to 40 W/cm^2, as shown in Fig. S2 (a). Because of the bubble dynamic contact angles, which can be differentiated as advancing and receding contact angles (α and β), are difficult to determine especially within the downstream region of the heated surface along the flow direction, and thus we only analyzed bubbles that form on the upstream surface (i.e. the red analytic region), which was not merged or affected by the neighboring bubbles. According to Fig. S2 (b), the measured results in terms of the averaged advancing and receding contact angles on the wettability-patterned surfaces were over a range of 50-120 and 40-80 degrees, respectively. In addition, it is widely known that the advancing contact angle is generally larger than the receding contact angle along the flow direction under flow boiling conditions. As such, three groups of advancing and receding contact angles (i.e. α/β=50/40, 60/50, and 70/60) were selected as representative cases for determining the relationship between the heat transfer coefficient (HTC) and the relative bubble lift force on surfaces composed of hydrophobic patterned arrays with various shapes.

Fig. S2 (c) shows HTC as a function of the predicted ratio of bubble lift force on wettability-patterned surfaces with various group of the advancing and receding contact angles, the predicted results indicated that the surfaces with the triangular shape revealed the highest ratio of bubble lift force than those with the inverted-triangular and circular shapes, which corresponded to the experimental results, indicating that bubbles can be released more frequently on surfaces with triangle hydrophobic patterns and subsequently improved the HTC. For preventing the overprediction on the bubble lift forces on the wettability-patterned surfaces, we selected the minimum predicted ratio of bubble lift force as the representative case by assuming that the advancing and receding around a single bubble on the wettability-patterned surfaces were 50 and 40 degrees, respectively in this study.

- **Added sentences in revised manuscript (page 16, line 1)**

"The basis of the assumption of bubble dynamic contact angles is given in the supplementary materials."

- **Added sentences in Supplementary material (page 2, line 1)**

"The assumption of the bubble dynamic contact angles was based on the bubble visualization results in this study, we analyzed single departing bubble from the surfaces consisted of the hydrophilic substrate and the hydrophobic patterned arrays in triangular, inverted-triangular, and circular shapes with the 1-mm inter-spacing, respectively as the heat flux raised to 40 W/cm^2, as shown in Fig. S2 (a). Because of the bubble dynamic contact angles, which can be differentiated as advancing and receding contact angles (α and β), are difficult to determine especially within the downstream region of the heated surface along the flow direction, and thus we only analyzed bubbles that form on the upstream surface (i.e. the red analytic region), which was not merged or affected by the neighboring bubbles. According to Fig. S2 (b), the measured results in terms of the averaged advancing and receding contact angles on the wettability-patterned surfaces were over a range of 50-120 and 40-80 degrees, respectively. In addition, it is widely known that the advancing contact angle is generally larger than the receding contact angle along the flow direction under flow boiling conditions. As such, three groups of advancing and receding contact angles (i.e. α/β =50/40, 60/50, and 70/60) were selected as representative cases for determining the relationship between the heat transfer coefficient (HTC) and the relative bubble lift force on surfaces composed of hydrophobic patterned arrays with various shapes.

Fig. S2 (c) shows HTC as a function of the predicted ratio of bubble lift force on wettability-patterned surfaces with various group of the advancing and receding contact angles, the predicted results indicated that the surfaces with the triangular shape revealed the highest ratio of bubble lift force than those with the inverted-triangular and circular shapes, which corresponded to the experimental results, indicating that bubbles can be released more frequently on surfaces with triangle hydrophobic patterns and subsequently improved the HTC. For preventing the overprediction on the bubble lift forces on the wettability-patterned surfaces, we selected the minimum predicted ratio of bubble lift force as the representative case by assuming that the advancing and receding around a single bubble on the wettability-patterned surfaces were 50 and 40 degrees, respectively in this study.

"

Added figure in Supplementary material

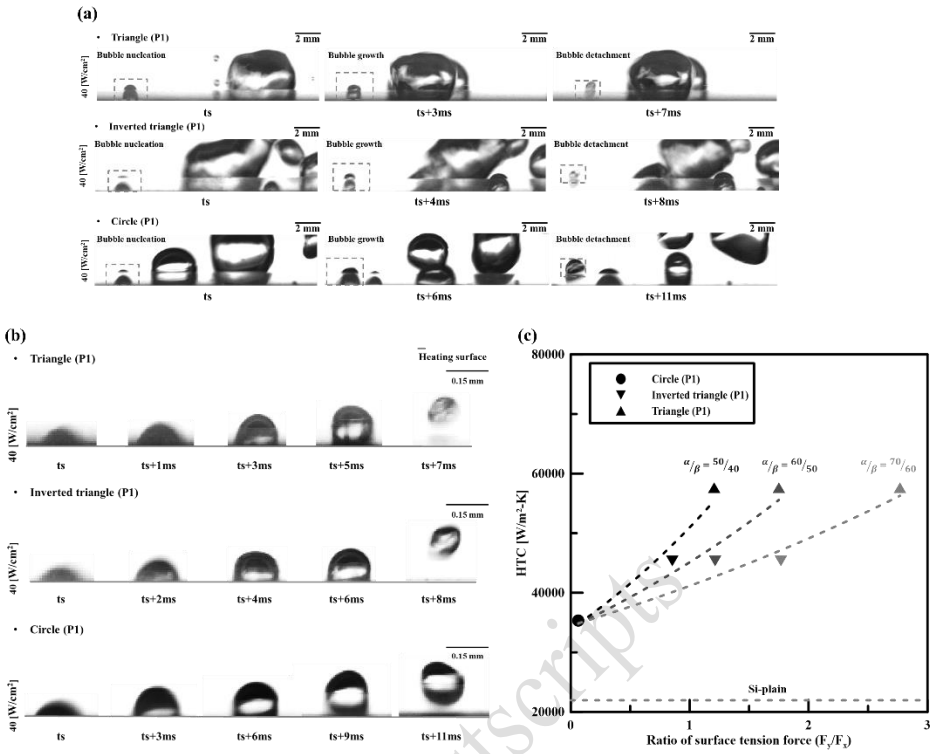

Figure S2 (a) Tracking regions of single departing bubble (b) Bubble detachment process and (c) HTC versus ratio of surface tension force on surfaces consisted of hydrophobic patterned arrays in triangular, inverted-triangular, and circular shapes with inter-spacing of 1 mm.

(8)

Test results of heterogeneous-wettability-patterned (this paper) and homogenous-wettability-patterned (Yin et al.) show the patterned surfaces can perturb the flow. Thus, they can enhance the flow boiling heat transfer. The authors should define the advantages of the heterogenous-wettability-patterned surface presented in this work by comparing it to the homogeneous-wettability-patterned surface results. Yin, Liaofei, et al. "Subcooled flow boiling in an expanding micro gap with a hybrid microstructured surface." International Journal of Heat and Mass Transfer 151 (2020): 119379.

(Reply)

As the reviewer commented, the advantages of the heterogeneous-wettability-patterned surface in the present study as compared to findings proposed by Yin et al. [25], who created homogeneous-hybrid surfaces consisted of rough surfaces and inverted-triangular pin-fin arrays (i.e., along the flow direction), for improving flow boiling heat transfer are concluded as follows:

1. The onset of nucleation boiling (ONB) can be triggered at low heat flux regions and subsequently improved the heat transfer coefficient (HTC) using hydrophobic islands on wettability-patterned surfaces.
2. For retarding a premature dry-out occurrence, the hydrophilic substrate can supply more coolant to the heated surface to prevent a rapid bubble coalescence and the premature dry-out, thus enhancing critical heat flux (CHF).
3. Both the homogeneous- and heterogeneous-wettability patterned surfaces can enhance the overall flow boiling heat transfer performance by perturbing the convective flow near heated surfaces, while bubbles might be released more efficiently on surfaces consisted of two wettability contrast regions because of the bubble slug flow can move faster by resulting in a "jump phenomenon" as the three-phase contact line reached the edge of hydrophobic patterns [Ref. 3].

- Revised sentences in revised manuscript (page 6, line 32)

"Additionally, in terms of homogeneous surfaces consisted of micro patterned arrays in flow boiling, Yin et al. [25] used an experimental method to investigated flow boiling heat transfer on hybrid surfaces consisted of rough regions and inverted-triangle pin-fin arrays, which vertically aligned in the downstream region, under subcooled conditions. Their experimental results showed that the pressure drop induced in the channel significantly decreased as using the hybrid surfaces even in a relatively high flow rate and large heat flux regions. On the other hand, the overall flow boiling heat transfer performance can be further improved using heterogeneous surfaces, by combining both advantages of hydrophobic and hydrophilic surfaces (i.e., bubble nucleation can be promoted on hydrophobic islands and a premature dry-out can be suppressed using hydrophilic substrates)."

- Added reference in revised manuscript

[25] Yin, L., Chauhan, A., Recinella, A., Jia, L. & Kandlikar, S. G. Subcooled flow boiling in an expanding microgap with a hybrid microstructured surface. International Journal of Heat and Mass Transfer 151 (2020), 119379.

- **Reference for revision**

[Ref. 3] Wang, H., Yang, Y., He, M. & Qiu, H. Subcooled flow boiling heat transfer in a microchannel with chemically patterned surfaces. International Journal of Heat and Mass Transfer 140 (2019), 587–597.